https://doi.org/10.5194/egusphere-2025-2314
Preprint. Discussion started: 30 May 2025

Relating extratropical atmospheric heat transport to cyclone life cycle characteristics and numbers in Southern Hemispheric winter

Jan Zibell[1], Alejandro Hermoso[2], Aaron Donohoe[3,4], and Sebastian Schemm[1,5]

[1]Institute for Atmospheric and Climate Science, ETH Zurich, Zurich, Switzerland
[2]Climate and Environmental Physics and Oeschger Centre for Climate Change Research, University of Bern, Bern, Switzerland
[3]Department of Atmospheric Sciences, University of Washington, Seattle, WA, US
[4]Applied Physics Laboratory, University of Washington, Seattle, WA, USA
[5]Department of Applied Mathematics and Theoretical Physics, Centre for Mathematical Sciences, University of Cambridge, Cambridge, UK

Correspondence: Jan Zibell (jan.zibell@env.ethz.ch)

Abstract.

Extratropical cyclones, which develop and propagate in regions known as storm tracks, account for the majority of poleward atmospheric heat transport (AHT) outside the tropics. This allows the intensity and position of the zonal mean storm track to be constrained by the hemispheric-wide radiative budget. Yet, the zonal mean nature of this approach masks the contribution of individual cyclones, which can locally constitute extreme eddy AHT. In this study, we adopt a cyclone-centered perspective to quantify in detail the relationship between poleward AHT and the life cycle characteristics of extratropical cyclones in Southern Hemispheric winter. Specifically, we combine objectively identified surface cyclone tracks derived from ERA5 data (1981–2021) with a moist static energy (MSE) framework that features an eddy-mean decomposition of the circulation. The eddy MSE flux maximizes during the cyclone intensification phase and is largest in the warm sector with a secondary maximum in the cold sector. Importantly, a considerable fraction of the flux in the warm-sector is located well equatorward of the cyclone center and thus outside the cyclonic region identified by the tracking algorithm. This leads to a latitudinal shift between maxima in cyclone frequency and eddy MSE fluxes. To bridge the gap between zonally integrated AHT and contributions from individual cyclones, local vertically integrated eddy MSE flux events are attributed to cyclones based on spatial overlap criteria. When integrating zonally and over the cyclone lifetime, the most intense cyclones (and not the ones intensifying most rapidly) generally exhibit the largest cyclone-attributed eddy MSE fluxes. Despite a disproportionate contribution to the cyclone-attributed eddy MSE fluxes by the most intense cyclones on the seasonal scale, the relationship between the seasonal number of intense cyclones and the poleward eddy MSE flux is sensitive to the choice of the eddy-mean decomposition. This result indicates that low wavenumber background flows mask the influence of cyclone characteristics in the vertical, zonal, and seasonal integral. Notably however, the relationship between the overall cyclone number and total AHT shows a peak at 50° S, which resembles the dominance of synoptic waves at this latitude in terms of AHT while the relevance of planetary waves increases poleward. Further research on the interplay between synoptic and planetary MSE fluxes in the vicinity of cyclones is

https://doi.org/10.5194/egusphere-2025-2314
Preprint. Discussion started: 30 May 2025

needed to understand to which extent the cyclone number, which is projected to decrease under warming, could be constrained by the global energy budget.

1 Introduction

Extratropical cyclones shape weather variability in the midlatitudes. In the Southern Hemisphere (SH), several extreme weather events have been linked to surface cyclones and their accompanying fronts such as South African cold spells (Chikoore et al., 2024) or flood events in Australia (Callaghan and Power, 2014). More generally, most extreme precipitation events in the extratropics can be related to extratropical cyclones (Pfahl and Wernli, 2012). Thus, understanding how the number and intensity of cyclones varies from year to year and will change under global warming is relevant for both immediate and long-term adaptation measures. It is well known that extratropical cyclones intensify in regions of large baroclinicity, i.e. where horizontal temperature gradients are large — for instance near a land-sea contrast or sea ice edge — and static stability is relatively low (e.g. Eady, 1949). These regions are also commonly referred to as storm tracks. In addition, individual storms can be strengthened by the release of latent heat during condensation within the ascent regions (e.g. Booth et al., 2013; Büeler and Pfahl, 2017). The circulation response to latent heating is non-linear and has been a matter of investigation for multiple decades (see the comprehensive review of Wernli and Gray, 2024, and references therein). Recent progress includes recognizing that latent heat release within a warm conveyor belt, which is the ascending moist airstream in the warm sector of a cyclone, can be linked to the amplification of the upper-level anticyclonic circulation downstream (Pomroy and Thorpe, 2000; Grams et al., 2011; Schemm et al., 2013; Steinfeld et al., 2020) and thereby the formation and maintenance of atmospheric blocking (Pfahl et al., 2015). The corresponding stationary flow can — depending on moisture availability — lead to further enhanced poleward moisture transport. One outstanding example where this self-amplifying poleward latent heat flux mechanism was identified is the March 2022 Antarctic heatwave: The extremely anomalous amount of moisture transported across the coastline into the continent led to the largest surface temperature anomaly (39 K) over the instrumental record (Blanchard-Wrigglesworth et al., 2023; Wille et al., 2024). Overall, cyclones in fact account for the dominant fraction of the latent heat fluxes into Antarctica (Tsukernik and Lynch, 2013) and, more generally, throughout the SH extratropics (Sinclair and Dacre, 2019).

Poleward latent heat fluxes make a vital contribution to the global meridional atmospheric heat transport (AHT), which moderates the equator-to-pole temperature gradient. Since Earth receives more solar energy in the tropics than at the poles and this equator-to-pole contrast in absorbed solar radiation is only partly compensated by gradients in emitted thermal radiation, the atmosphere and ocean must collectively transport energy poleward to counteract the net radiative energy imbalance (Peixoto and Oort, 1992). AHT is described by the flux of moist static energy (MSE), which is the sum of latent and dry heat. The MSE flux can be related to different time-scales and length-scales such that total AHT is commonly separated into eddy and background flux contributions, which are typically assessed in the zonal mean (e.g. Priestley, 1949; Barpanda and Shaw, 2017). In midlatitudes, high-frequency synoptic-scale eddies are the largest contributors to AHT in both hemispheres (e.g. Armour et al., 2019; Stoll et al., 2023). Adding to that are low-frequency stationary waves and the mean overturning circulation; the latter corresponding to the Ferrell cell transporting heat equatorward in the midlatitudes.

https://doi.org/10.5194/egusphere-2025-2314
Preprint. Discussion started: 30 May 2025

Different flow decompositions and definitions of storm tracks have led to various insights on their dynamics: Defining storm tracks using the zonal mean high-frequency eddy MSE flux, for instance, allows seasonal and climatological changes in storm track intensity and latitude to be related to large scale energetic constraints on total AHT alongside information about the AHT by the stationary circulation (Barpanda and Shaw, 2017; Shaw et al., 2018). Moreover, decomposing AHT by spatial scale has enabled a link between zonal mean MSE flux extremes and localized weather patterns (Lembo et al., 2022). These studies are examples for what can be classified as a kind of 'top-down' approach to connect the zonal mean AHT to local weather phenomena. Conversely, the corresponding 'bottom-up' approach that investigates how local eddy MSE flux extremes impact the zonally integrated AHT has also been studied extensively. On the one hand, (extreme) eddy MSE fluxes have been linked to the warm- and cold-sectors of midlatitude cyclones (Messori and Czaja, 2015; Messori et al., 2017), which majorly contribute to the zonal mean eddy MSE flux (Messori and Czaja, 2013). In addition, days with enhanced zonal mean eddy MSE fluxes have a disproportionate impact on the seasonal integral (Messori and Czaja, 2015) suggesting that local extreme events may significantly contribute to climatological zonal mean flux. On the other hand, it was found that local flux extremes arise from a combination of synoptic and planetary signals (Messori and Czaja, 2014). This indicates that eddy MSE fluxes in the vicinity of a cyclone might not solely be determined by its life cycle characteristics but also contain contributions from low-frequency background flows. Despite the advances from both 'top-down' and 'bottom-up' approaches, a systematic quantification how individual cyclones contribute to AHT over their life cycle and how the cyclone number and intensity over a season are related to eddy MSE flux (and thereby more generally the total AHT) has not been performed thus far.

Further motivation for this study arises from the conception that the atmospheric energy budget might impose a constraint on the number of extratropical cyclones. In a warmer climate, for instance, eddy latent heat fluxes in the warm sectors of cyclones increase — even if the circulation in the eddy were unchanged — simply due to the Clausius-Clapeyron relationship (Geen et al., 2016). Assuming for simplicity that the equator-to-pole gradient in net radiative imbalance (and the ocean heat transport) were unchanged (Boer and Sargent, 1985), this would require total AHT to be unchanged as well. Given that high-frequency eddy MSE fluxes remain the dominant component of extratropical AHT (especially in SH winter, Donohoe et al., 2020), the required total AHT could be achieved by fewer cyclones each transporting more latent heat (Zhang and Wang, 1997). Apart from few exceptions (Chang et al., 2012), there is agreement based on various warming scenarios, models, and approaches to cyclone counting that the SH cyclone number decreases in a warmer climate (König et al., 1993; Geng and Sugi, 2003; Lambert and Fyfe, 2006; Grieger et al., 2014; Chang, 2017; Priestley and Catto, 2022). Highly idealized atmosphere-only experiments underpin this response to warming (Sinclair et al., 2020; Schemm et al., 2022). However, the relationship between the extratropical cyclone number and AHT is complicated by the fact that the eddy MSE transported by individual cyclones likely depends on the cyclone characteristics such as the spatial extent. On the one hand, the Rossby radius of deformation — an estimate for typical eddy size — is expected to respond to changes in static stability and tropopause height (Gill, 1982). On the other hand, strongly diabatically-driven cyclones become smaller under warming (Booth et al., 2013). Thus, how the partitioning of the total eddy MSE fluxes onto extratropical cyclones is affected by warming is non-trivial. Further complexity arises from possible changes in ocean heat uptake and transport in the Southern Ocean which may buffer the atmospheric response to changes in radiative forcing and enhanced atmospheric latent heat storage.

https://doi.org/10.5194/egusphere-2025-2314
Preprint. Discussion started: 30 May 2025

Addressing the storm track response to climate forcing necessitates a more profound understanding of the relationship between zonal mean AHT and cyclone number and intensity under current climate conditions. In this study, we aim to bridge the gap between the synoptic-scale cyclone and zonal mean AHT perspectives by investigating 41 years of reanalysis data. Firstly, the spatio-temporal relationship between meridional eddy MSE fluxes and extratropical cyclones is explored. Building on that, we inspect the contribution of a cyclone to the zonally integrated, meridional eddy MSE flux — in other words its energy footprint — by introducing a feature-based approach to attribute eddy MSE fluxes to individual cyclones. While trends in AHT (and its sub-components) have been investigated in previous studies (Rydsaa et al., 2021; Clark et al., 2022; Simmons, 2022; Franzke and Harnik, 2023; Cox et al., 2024a; Kang et al., 2024), we examine the inter-annual variability of the seasonal cyclone number along with seasonal eddy MSE fluxes. The specific research questions thus are:

- How does the eddy MSE flux evolve in the vicinity of surface cyclones in the SH during their life cycle?
- Are different cyclone characteristics, in particular intensification rate and intensity, reflected differently in the zonally integrated energy flux, and if so, how?
- On a seasonal scale, how is the number of cyclones related to eddy MSE flux, and more generally the total AHT?

We focus on the SH storm track during the winter months June, July, and August (JJA). In contrast to the Northern Hemisphere (NH), the SH storm track is nearly circumpolar and therefore more zonally symmetric, which simplifies linking zonal mean fluxes to cyclone characteristics. Moreover, winter is the season during which cyclone activity is maximum. The methods applied in this study are detailed in Sect. 2. The evolution of eddy MSE fluxes along cyclone life cycles, including spatial composites, is presented in Sect. 3. How cyclone characteristics influence the energy footprint of a cyclone in the zonal integral is shown and discussed in Sect. 4. The seasonal relationship between (eddy) AHT and extratropical cyclone number is examined in Sect. 5. Finally, the results are summarized and put into a broader context in Sect. 6.

2 Methods

2.1 Reanalysis data

This study discusses extratropical dynamics during the winter season in the ERA5 reanalysis data set (Hersbach et al., 2020), which corresponds to JJA in the SH. The analyses are based on six-hourly data of the years 1981 to 2021. All variables are obtained at $0.5° \times 0.5°$ resolution and MSE fluxes are computed at 28 of the 37 available pressure levels spanning 1–1000 hPa. This vertical coarsening has minimal impact on the monthly closure of the energy budget (see Sect. 2.3, Eq. 1).

2.2 Cyclone tracking

Extratropical cyclones are identified using the cyclone tracking algorithm developed by Wernli and Schwierz (2006) and refined by Sprenger et al. (2017). Local minima of sea level pressure (SLP) are identified and followed over time. The spatial extent of each of these identified cyclones is then defined using a closed SLP contour approach. The outermost SLP contour around

https://doi.org/10.5194/egusphere-2025-2314
Preprint. Discussion started: 30 May 2025

a SLP minimum which is shorter than $7500\,\mathrm{km}$ encircles the cyclone area. Flagging gridcells within this area thus yields a cyclone mask. The lifetime of a track is defined as the length of each track while intensity (and intensification) are defined by the center SLP (and its change). While cyclones are tracked using hourly SLP input, only six-hourly time steps are considered in the analysis to match the temporal resolution of the calculated MSE fluxes. Tracks that are shorter than $24\,\mathrm{h}$, weaker than $990\,\mathrm{hPa}$, and intensify equatorward of $30°$ are discarded. Furthermore, we exclude tracks that do not intensify based on the maximum SLP tendency normalized with $\frac{\sin 60°\mathrm{S}}{\sin \phi}$ with the cyclone center at latitude ϕ (Sanders and Gyakum, 1980). Thus, we filter out tracks that intensify less than $0\,\mathrm{Bergeron}$. As a reference, $1\,\mathrm{Bergeron}$ corresponds to a deepening rate of $24\,\mathrm{hPa\,h^{-1}}$ at $60°$ S. These criteria are applied to discard thermal lows that originate and disappear with the daily cycle, tropical cyclones that do not undergo extratropical transition, and cyclones that remain very weak. For comparability of different MSE flux decomposition methods, a track is not included in a composite if the considered stage falls onto a leap day.

2.3 MSE fluxes

A simplified version of the vertically integrated and zonally averaged atmospheric energy balance reads

$$\partial_t \langle [h] \rangle + \partial_y \langle [vm] \rangle = [F_{\mathrm{TOA}} - F_{\mathrm{S}}] \tag{1}$$

(Neelin and Held, 1987; Barpanda and Shaw, 2017). $h = c_p T + Lq$ corresponds to the thermal energy within the atmospheric column and $m = c_p T + Lq + \Phi$ the MSE with c_p being the specific heat capacity of air, L the latent heat of evaporation, T and q air temperature and specific humidity, respectively, and Φ the geopotential. v denotes meridional wind. F_{TOA} and F_{S} represent the net energy flux at the top of atmosphere (TOA) and surface, respectively. F_{TOA} is comprised of only radiative fluxes whereas F_{S} includes both radiative and turbulent fluxes. $\partial_y(\cdot) \equiv \partial_\phi\{\cos\phi(\cdot)\}/(a\,\cos\,\phi)$ is the meridional divergence and $\langle\cdot\rangle \equiv \frac{1}{g}\int_{\overline{p_S}}^{0}(\cdot)dp$ the mass-weighted vertical integration from the climatological mean surface pressure $\overline{p_S}$ to the TOA (Boer and Sargent, 1985). Note that this formulation neglects kinetic energy and latent heat related to the liquid-ice transition (Mayer et al., 2024) and defines the energy tendency relative to a fixed mass of atmosphere following Cox et al. (2024b).

We further decompose the MSE flux into eddy and mean components. One established approach defines eddies from monthly means, such that the monthly mean flux reads

$$[\overline{vm}] = \underbrace{[\overline{v'm'}]}_{\mathrm{TE}} + \underbrace{[\overline{v}^*\overline{m}^*]}_{\mathrm{SE}} + \underbrace{[\overline{v}][\overline{m}]}_{\mathrm{MOC}} \tag{2}$$

with dashes and asterisks signifying anomalies from the monthly $\bar{\cdot}$ and zonal averages $[\cdot]$, respectively (Priestley, 1949; Peixoto and Oort, 1992). Here we adopt the interpretation of the terms on the right-hand side from Barpanda and Shaw (2017): the terms denoted with TE and SE represent transient and (temporally) stationary eddies, respectively, whereas the third term corresponds to the meridional overturning circulation (MOC). Note that vertical averages of m and v are subtracted before computing the MOC (Marshall et al., 2014) to account for mass conservation — *MSE* fluxes associated with a net *mass* flux are noisy and do not correlate strongly with the corresponding mass changes of the polar cap (Cardinale et al., 2021). This study focuses on the TE fluxes which are thought to be related to synoptic weather systems (e.g. Kaspi and Schneider, 2013;

https://doi.org/10.5194/egusphere-2025-2314
Preprint. Discussion started: 30 May 2025

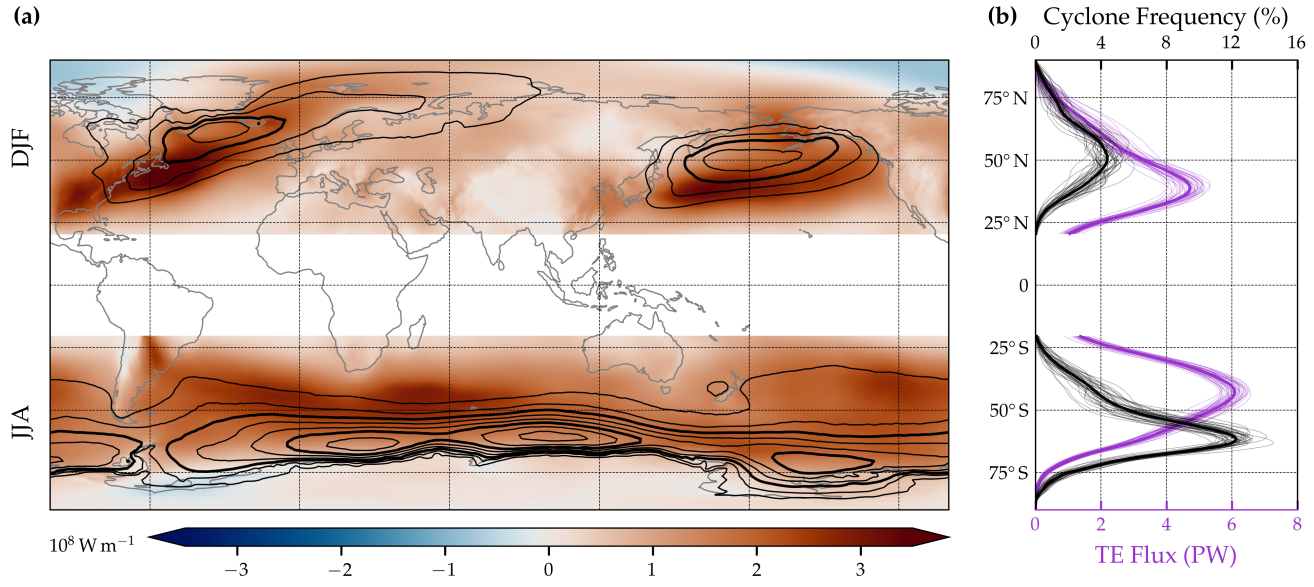

Figure 1. Climatologies of TE MSE fluxes and cyclone frequencies during winter. **(a)** Vertically integrated and seasonally averaged TE MSE fluxes, $\langle \overline{v'm'}_{\mathrm{TE}} \rangle$, (shading) are shown along with the cyclone mask frequency (black contours in steps of 5 % starting at 5 % with 15 % and 30 % highlighted in thicker contours). **(b)** Zonally integrated TE MSE fluxes, $\langle [\overline{v'm'}_{\mathrm{TE}}] \rangle$, (purple) and zonal mean cyclone frequencies (black) for individual seasons (thin lines) and the climatology thereof (solid lines). For compactness and better comparability, MSE fluxes are shown positive poleward in this panel. Note that the cyclone frequency in **(b)** is multiplied with the cosine of latitude for consistency with the zonally integrated poleward energy fluxes. In both **(a, b)**, values in the NH are for DJF and JJA in the SH, while latitudes near the equator are masked.

Barpanda and Shaw, 2017). Hereafter, we will refer to the TE fluxes calculated in this framework with $v'm'_{\mathrm{TE}}$. The NH DJF and SH JJA climatologies of vertically integrated $v'm'_{\mathrm{TE}}$ are shown in Fig. 1. Throughout this study, fluxes in each hemisphere are defined positive if poleward. Climatologically, the maximum fluxes (shading in Fig. 1a) are located equatorward of the storm tracks (surface cyclone frequency in black contours). Zonally integrating (eddy) AHT involves a multiplication with a cosine of latitude and we present the cosine latitude weighted cyclone frequency in Fig. 1b to account for the changing area per grid cell and remain consistent with the definition of AHT. Seasonally averaged fluxes (purple lines in Fig. 1b) in the SH amount to 6 PW with the difference between the weakest and the strongest season being roughly 1 PW at 45° S.

The above boxcar approach to monthly averaging in the 'TE framework' leads to somewhat unphysical discontinuities at the turn of each month. Also, the window-length of around 30 d is to some extent arbitrary and arguably unrelated to the synoptic timescales of interest. Most results are based on large cyclone sample sizes such that the introduced methodological biases are assumed to average out. We use two additional MSE flux decomposition methods for to explore the sensitivities of the results. One of the most widely used approaches in weather science to separate eddy and background signals is a decomposition into high-pass and low-pass filtered components (e.g. Hoskins et al., 1983; Schemm and Rivière, 2019; Franzke and Harnik, 2023).

https://doi.org/10.5194/egusphere-2025-2314
Preprint. Discussion started: 30 May 2025

While closing the energy budget using such an approach can require computing many cross-terms (Franzke and Harnik, 2023), we simply compare $v'm'_{\mathrm{TE}}$ to the eddy flux signal, $v'm'_{\mathrm{HP}}$, where dashes denote the high-pass (HP) components. v and m are concatenated for the entire analysis period (only ignoring leap days) and high-pass filtered with a frequency cut-off at 10 d.

The third method that is used for sensitivity tests defines eddy fluxes via anomalies from zonal means *instantaneously* (Cox et al., 2024b). In contrast to the other two methods, no timescale is introduced in this decomposition method. The eddy fluxes derived from zonal anomalies (ZA) are referred to as $v^*m^*_{\mathrm{ZA}}$. These local eddy fluxes depend on the flux that occurs elsewhere at the same latitude, whereas for the other methods the eddy flux depends on the local flux evolution in time.

2.4 Cyclone composites

Going beyond the zonal mean, eddy MSE fluxes are inspected in the vicinity of cyclone centers by the use of composites. For a given set of cyclones (including all or only the deepest ones, for instance) and stages (e.g. time of maximum intensification), nearby eddy MSE fluxes are regridded such that the cyclone center is located at (0,0) in cyclone-centered longitude and latitude coordinates. Bilinear interpolation is chosen for all fields except for precipitation where conservative remapping conserves the peaks. Note that unlike other studies (e.g. Catto et al., 2010; Dacre et al., 2023), the resulting fields are *not* rotated along track direction. Rotated coordinates are usually preferred to retain and highlight separate signals from warm and cold fronts. However, when investigating meridional energy fluxes we chose to conserve the direction of flux within the composite. Grid-points falling below climatological surface pressure (which approximates the topography) have been masked out for the composites.

2.5 Attributing eddy MSE fluxes to cyclones

The composite analyses based on the complete eddy MSE flux fields in Sect. 3.2 reveal that substantial fluxes are located further away from the cyclone center and outside of the largest closed SLP contour (which the cyclone mask is derived from). Instead of using the cyclone masks to attribute eddy MSE fluxes to the cyclones, we identify and attribute to the cyclone eddy MSE fluxes (which can be outside of the mask) that are thought to be associated with the cyclone-induced circulation. There is no single correct approach to identify coherent features in atmospheric flows (see, for instance, a comparison of atmospheric river tracking algorithms in Shields et al., 2018). In this work, flux features are identified using a flux threshold based on a percentile which broadly resembles the spirit of the approach of Messori et al. (2017). Since especially MSE is varying greatly with season and latitude, the flux threshold is chosen to be latitude- and time-dependent. This is achieved by taking a percentile of all values of a latitude band at the same time step of each year (resulting in $360° \;/\; \Delta_{\mathrm{lon}} \cdot \mathrm{N}_{\mathrm{years}} = 29520$ values to draw the percentile from, see Fig. B1) at each latitude and timestep.

Given a percentile rank p, features of the vertically integrated flux $\langle v'm'_{\mathrm{TE}} \rangle$ are identified using the flux thresholds corresponding to p for northward fluxes and $100\,\% - p$ for southward fluxes with $p > 50\,\%$. The resulting MSE flux features that are larger than $4.9{\cdot}10^4\,\mathrm{km}^2$ (about $1° \times 1°$) and poleward of 15° are then labeled using `TempestExtremes v2.1` (Ullrich et al., 2021). Instead of tracking (or "stitching" in the language of the tool) the resulting flux features over time, the eddy MSE flux features that spatially overlap the SLP masks are attributed to unique cyclones at each time step. Non-overlapping features are considered 'other' eddy fluxes (see Fig. B2). If a flux feature overlaps with multiple cyclones, the cyclone with lowest

https://doi.org/10.5194/egusphere-2025-2314
Preprint. Discussion started: 30 May 2025

center SLP at that time step is chosen. Choosing from the overlapping cyclones randomly instead was also tested but makes no qualitative difference on the results in this paper. Therefore, we think that a more sophisticated algorithm that tracks flux features which are then attributed to cyclones based on some evolution criteria would not lead to markedly different results. Note that given the percentile rank p, the ratio of grid points attributed to cyclones is not exactly $2 \cdot (100\,\% - p)$ ('northward' plus 'equatorward' areas) but less because small features are filtered out and not all of the remaining are attributed to cyclones. The results in Sects. 4 and 5 are for $p = 90\,\%$. Two other percentile ranks $p = 80\,\%$ and $p = 95\,\%$ have been tested which tend to attribute broader and narrower features to the cyclones, respectively.

3 Eddy MSE fluxes along extratropical cyclones

This first result section starts addressing the relationship between TE MSE fluxes and extratropical cyclones by investigating the evolution of $v'm'_{\mathrm{TE}}$ along the typical cyclone life cycle. The adopted cyclone-centered perspective allows for a better understanding of how $v'm'_{\mathrm{TE}}$ co-locates with cyclone centers, changes along cyclone life cycle, and relates to cyclone intensification. The life cycle analyses and cyclone-centered composites complement and expand on previous research aggregating eddy MSE flux events based on flux magnitude. Special attention is paid to the partitioning into dry and moist flux components in the warm and cold sectors across different latitudes. As indicated, the following results are based on calculating eddy MSE fluxes using the TE framework — from anomalies defined as departures from the monthly mean. 4 and 5.

3.1 Eddy MSE flux along the cyclone life cycle

To obtain an impression of the evolution of a variable along the cyclone life cycle, it has proven helpful to consider normalized cyclone tracks (e.g. Rudeva and Gulev, 2007; Schemm et al., 2018): For the first analysis, tracks are split into a deepening and a weakening phase. All tracks that feature more than two time steps in both of these phases are then normalized for both periods [genesis, mature stage] and [mature stage, lysis] separately. Any quantity can be interpolated onto the resulting, uniform x-axis using cubic spline interpolation (Fritsch and Carlson, 1980; Schemm et al., 2018).

This approach is applied to the maximum $850\,\mathrm{hPa}$ $v'm'_{\mathrm{TE}}$ within a $7.5°$ radius from the cyclone center. Considering *all* SH cyclones, the maximum $v'm'_{\mathrm{TE}}$ features a peak before mature stage and declines afterwards (black line in Fig. 2).[1] The peak flux during intensification phase is, on average, around $50\,\%$ larger than towards the end of the deepening phase. The maximum TE MSE flux peaking before mature stage is consistent with the baroclinic life cycle whereby eddy heat flux peaks while baroclinicity is being eroded and intensification terminates (Novak et al., 2015). Certainly, computing the maximum flux within a fixed radius from the center introduces the possibility of capturing the signal of another cyclone at a different stage. Thus, for larger radii fluxes before and after mature stage increase uniformly (not shown). Moreover, both lifetime and latitude of this large set of SH cyclones span broad ranges. This motivates studying cyclone subsets as done throughout the remainder of the section.

[1] This is verified by centering the tracks onto the stage of peak intensification or mature stage without performing the spline interpolation and using different radii (not shown).

https://doi.org/10.5194/egusphere-2025-2314
Preprint. Discussion started: 30 May 2025

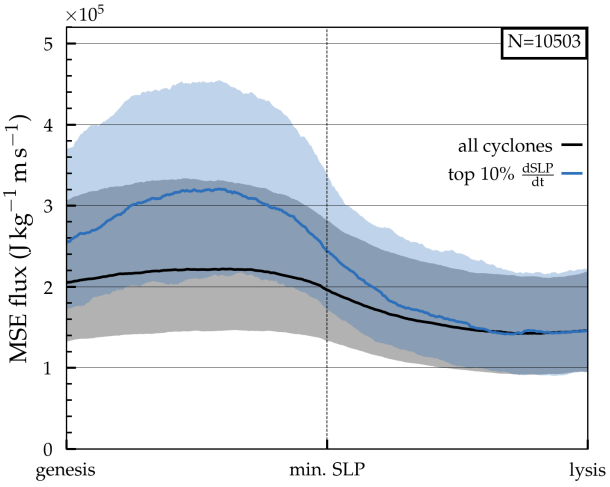

Figure 2. Maximum near-cyclone TE MSE flux, $v'm'_{\mathrm{TE}}$, at 850 hPa for all (black) and the 10 % most strongly intensifying cyclones (blue) along the normalized cyclone life cycle. The search radius is 7.5°. Median and interquartile range are shown in solid lines and shading, respectively. Genesis and lysis correspond to the first and last time steps of the track, respectively, while the mature stage is defined as the time of minimum central SLP. For track normalization, a cubic spline fit is performed for each track and the resulting distribution. The number of all SH cyclones is included in the upper right.

With fluxes peaking during the intensification phase, it is natural to ask whether the magnitude of the intensification rate plays a role for the magnitude of the nearby fluxes. Indeed, the above TE MSE flux contrast before and after mature stage is even larger when considering the subset of the 10 % most strongly intensifying cyclones (blue line in Fig. 2). The median flux of this subset is roughly 50 % larger during the intensification phase compared to *all* SH cyclones, but levels off after mature stage to comparable values of *all* SH tracks towards lysis. The difference of median flux during intensification and deepening amounts to a factor of around two. As above, near-cyclone $v'm'_{\mathrm{TE}}$ has been weakening again when mature stage is reached. Therefore, the following analyses will focus solely on the deepening phase.

3.2 Spatial relation of eddy MSE fluxes and cyclones

Next, cyclone-centered composites are inspected to study how fluxes are distributed around the cyclone center and occur spatially along the cyclone life cycle. Recall that in the SH, cyclonic flow is *clockwise* and that *poleward* flux is chosen *positive* in this study. Also note that the poleward transport of (temporally) anomalously warm and moist and the equatorward transport of anomalously cool and dry air both have positive poleward MSE and, thus, both the warm and cold sectors show positive MSE fluxes.

Composites of *all* SH cyclones indicate poleward $v'm'_{\mathrm{TE}}$ downstream of the cyclone center during genesis and peak intensification at 850 hPa (Fig. 3a, b). Note that the signal at the genesis stage in Fig. 3a is partly due to secondary cyclogenesis along the cold front leading to cyclones 'inheriting' fluxes from previous, still intensifying ones. During mature stage, this signal is

https://doi.org/10.5194/egusphere-2025-2314
Preprint. Discussion started: 30 May 2025

located further downstream and accompanied with an emerging negative (equatorward) flux upstream of the cyclone center at $(-1°, 0°)$ in the composite coordinates. Further upstream, a positive signal related to the cold sector only stands out towards the mature stage (Fig. 3c). From vertical cross-sections across $\mathrm{rlat} = 0$, i.e. the latitudinal band through the center, it becomes clear that the signal of the warm sector extends up to roughly $300\,\mathrm{hPa}$ during all considered stages with a peak around $900\,\mathrm{hPa}$ (Fig. 3d–f). This generally agrees with the vertical extent when centering around $850\,\mathrm{hPa}$ MSE flux extremes (Messori and Czaja, 2015). Thus, the signal in the warm sector is the footprint of the ascending warm and moist airstream known as warm conveyor belt. Likewise, the flux in the cold sector at mature stage maximizes at that level. The aforementioned negative signal located upstream of the cyclone center extends up to around $700\,\mathrm{hPa}$ while around $500\,\mathrm{hPa}$ a negative signal downstream of the center appears (Fig. 3f). A significance test supports that these fluxes that we relate to cyclonic flow features are different from climatology (see Sect. C, Fig. C1).

Composite mean meridional winds (grey lines in Fig. 3d–f) tilt westward with height during genesis and intensification but become more barotropic at mature stage.[2] Conceptually, this vertical velocity tilt matches the characteristic of the most unstable, fastest-growing perturbation in the Eady model (Eady, 1949). Likewise, the more barotropic flow at mature stage represents the end of baroclinic growth. Temperature anomalies (which dominate MSE anomalies), in turn, are expected to tilt eastward with height (Eady, 1949), which was confirmed for the composite MSE anomalies (not shown). The negative flux signal during mature stage at $500\,\mathrm{hPa}$ results from cold air moving poleward (Fig. 3f). Furthermore, the low-level equatorward flux at mature stage can be related to warm and moist air flowing equatorward along the bent-back extension of the warm front (Shapiro and Keyser, 1990). This signal does not emerge when centering on flux extremes but highlights the importance and value of the cyclone life cycle perspective.

The composite analysis confirms the previous findings based on normalized tracks that meridional TE MSE fluxes near cyclones are, on average, largest during the intensification phase. Likewise, from a spatial composite perspective, the flux of the $10\,\%$ most strongly intensifying cyclones is roughly $50\,\%$ larger in the cold sector, but up to $80\,\%$ larger in the warm sector close to the cyclone center as compared to *all* SH cyclones (compare, for instance, Fig. 4a to Fig. 3b at $850\,\mathrm{hPa}$). Differing percentage increases between the along-track evolution and composite map perspectives likely arise from applying a fixed radius to search for a maximum in the former method and varying lifetimes being aggregated (as discussed above). Strongly intensifying cyclones feature negative fluxes at $300\,\mathrm{hPa}$ downstream of the center which can be related to the anticyclonic return flow of the warm conveyor belt and which are less prominent in the composites of *all* SH cyclone (compare Fig. 4c and Fig. 3e).

We want to note that selecting for the tracks with deepest SLP instead of those deepening most strongly does not qualitatively impact the above conclusions. Both warm and cold sector signals are slightly more horizontally and vertically extended with the warm sector peak slightly reduced (at peak intensification, Fig. 4b, d). This points toward deep cyclones not necessarily being the ones intensifying most strongly but being larger in size (Rudeva and Gulev, 2007).

While these results suggest that near cyclones, $v'm'_{\mathrm{TE}}$ is largest in the warm sector, for some cyclones fluxes may also be large in cold sectors. Previous research has shown that poleward transport extremes can be both related to warm air moving

[2]While v' is shown in Fig. 3, this is also the case for the full meridional wind v (Fig. C1).

https://doi.org/10.5194/egusphere-2025-2314
Preprint. Discussion started: 30 May 2025

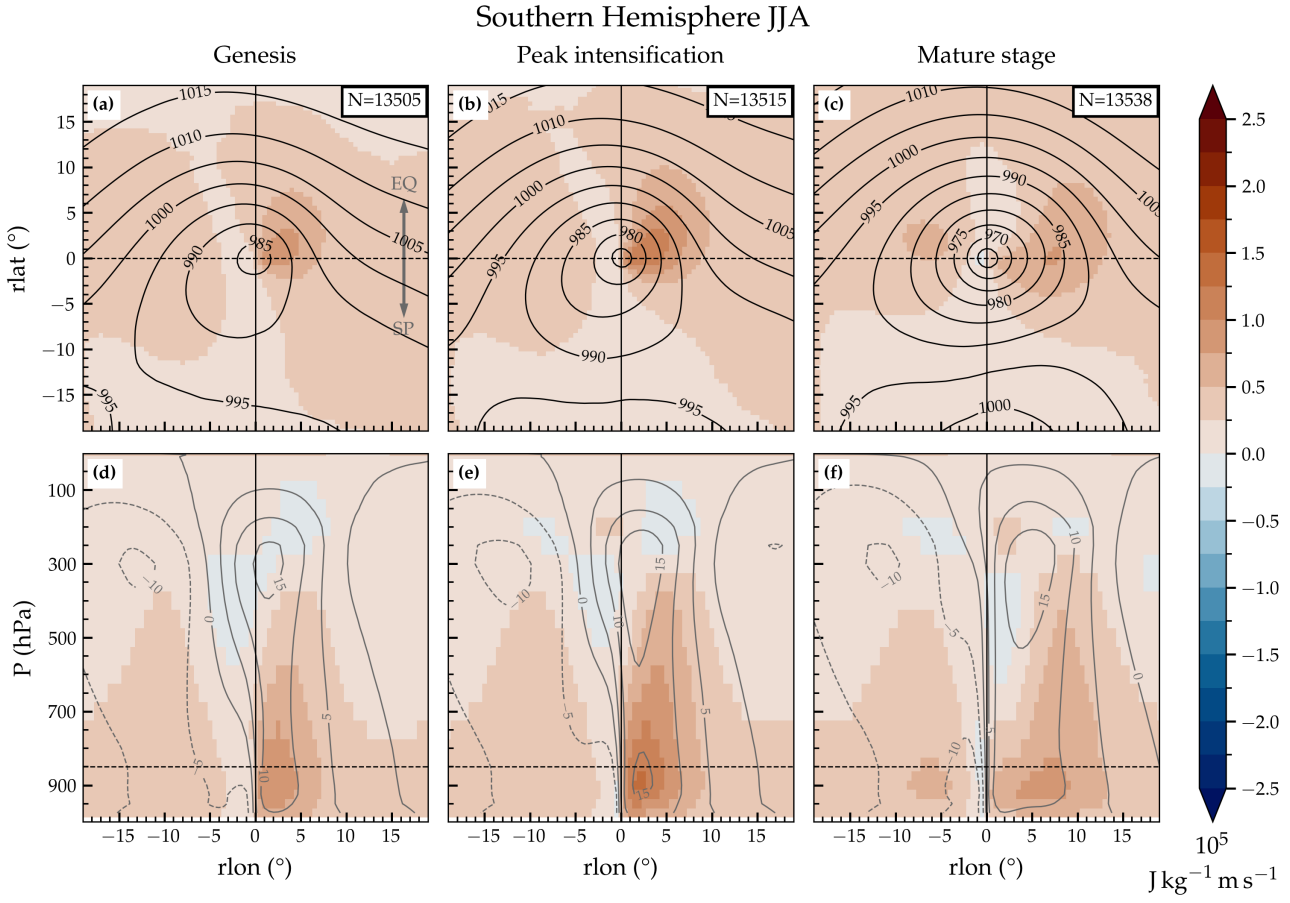

Figure 3. Cyclone-centered meridional TE MSE flux, $v'm'_{\mathrm{TE}}$, composited for different stages along the cyclone life cycle. Horizontal maps are shown for fluxes (colors) at 850 hPa for **(a)** genesis, **(b)** time of peak intensification, and **(c)** mature stage. Black contours indicate composite mean SLP in hPa. Similarly, height-longitude cross-sections through $\mathrm{rlat} = 0$ are shown in panels **(d)–(f)** for the same stages as in **(a)–(c)**. Grey lines depict meridional wind velocities (v') in $\mathrm{m\,s^{-1}}$ (positive poleward). Horizontal dashed black lines represent the intersection of the corresponding vertical and horizontal panels. Furthermore, the number of cyclones in the composites are included in the upper right in panels **(a)–(c)**. A grey arrow is included for better orientation indicating directions of equator (EQ) and South Pole (SP).

poleward as well as equatorward cold air advection. Both of these 'flavors' of poleward heat transport can be associated with $v'm'_{\mathrm{TE}}$ of comparable magnitude (Messori and Czaja, 2015). Furthermore, banded structures of the latter account for around 40 % of poleward heat transport across a wide range of latitudes (Messori et al., 2017). Thus, the lack of a signal upstream of
280 the cyclone center that is comparable to the one found in the warm sector might be surprising.

We expect this warm-cold sector flux contrast in our composites to arise for several reasons. Firstly, a simple geometrical explanation for this contrast can be seen when assuming the wind field in geostrophic balance with the SLP contours ($v = (f\rho_A)^{-1}\, dp/dx$ with f the Coriolis parameter, ρ_A air density, p pressure, and x longitude). When inspecting the latitude of

https://doi.org/10.5194/egusphere-2025-2314
Preprint. Discussion started: 30 May 2025

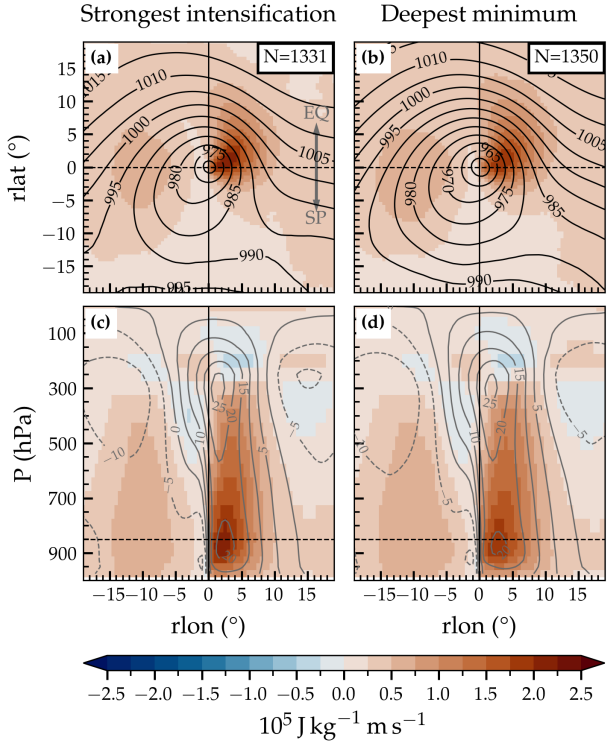

Figure 4. Cyclone-centered TE MSE flux at 850 hPa composited during time of peak intensification for **(a)** the 10 % most strongly intensifying cyclones and **(b)** the 10 % deepest cyclones at mature stage. Black contours indicate composite mean SLP in hPa. As in Fig. 3, horizontal maps are complemented with height-longitude cross-sections in panels **(c, d)**. Grey lines depict meridional wind velocities (v') in $\mathrm{m\,s^{-1}}$ (positive poleward). Horizontal dashed black lines represent the intersection of the corresponding vertical and horizontal panels. Furthermore, the number of cyclones in the composites are included in the upper right in panels **(a, c)**. A grey arrow is included for better orientation indicating directions of equator (EQ) and South Pole (SP).

the cyclone center (dashed horizontal line) in Fig. 3b, for instance, one can see that the contours of SLP are almost perfectly meridionally oriented downstream of the center but contain an additional zonal component upstream (in other words the upstream SLP contours resemble a bottom-left to top-right tilt on the panel). Therefore, v is larger in the warm sector and, thus, $v'm'_{\mathrm{TE}}$ would be expected to be larger in the warm sector even if the winds in both sectors were advecting the same magnitude MSE gradient. This is an important caveat of focusing only on meridional TE MSE fluxes.

Secondly, in particular during the intensification phase fronts are located relatively close to the cyclone center (Schemm et al., 2018) and only detach when an occlusion forms at a later stage of the life cycle (Shapiro and Keyser, 1990). The warm sector is spatially bound by the warm and cold fronts and narrows towards mature stage and lysis as the cold front catches up the warm front. Compositing by the cyclone center implies a tendency to centering next to the warm sector especially during

https://doi.org/10.5194/egusphere-2025-2314
Preprint. Discussion started: 30 May 2025

the intensification phase. Conversely, the upstream extent of the cold sector is generally not limited by frontal zones and hence can be more smeared out in the composite.

Thirdly, moisture causes the warm sector eddy MSE fluxes to be greater than those in the cold sector. At low levels such as $850\,\mathrm{hPa}$, latent heat in the warm sector adds to MSE while cold sectors are much drier (Messori and Czaja, 2015; Geen et al., 2016; Messori et al., 2017). In addition to its mere presence, if calculated as anomalies from a mean of a sample (such as monthly mean or zonal mean), positive specific humidity anomalies are even larger than negative ones because the spatiotemporal distribution of specific humidity is skewed — due to the non-linear Clausius-Clapeyron relationship, specific humidity increases exponentially with the temperature in a warm sector under constant relative humidity — and has a lower bound.

3.3 Latitudinal variations of dry and latent eddy heat fluxes

Of course, specific humidity, q, and thereby the contribution of latent heat flux to MSE flux is highly dependent on temperature and therefore also latitude. In the following, the above set of $10\,\%$ most strongly intensifying cyclones are sorted into $10°$ latitude bands according to the cyclone center latitude at time of peak intensification.

Downstream of the cyclone center, both $v'm'_{\mathrm{TE}}$ and $v'Lq'_{\mathrm{TE}}$ decrease towards the pole (Fig. 5). Unlike $v'm'_{\mathrm{TE}}$, $v'Lq'_{\mathrm{TE}}$ is confined to the warm sector downstream of the center which is in line with the arguments above. Notably, going towards the pole the decrease in $v'm'_{\mathrm{TE}}$ in the cold sector is less pronounced than in the warm sector such that the contrast between warm and cold sectors almost vanishes for cyclones intensifying within 60–$70\,°\mathrm{S}$ (Fig. 5c). This points to a larger relative importance of cold air outbreaks to the energy budget towards the high latitudes (Messori et al., 2017).

Not only the magnitude of $v'Lq'_{\mathrm{TE}}$ but also the relative contribution to $v'm'_{\mathrm{TE}}$ reduces towards pole (black contours in Fig. 5a–c corresponding). Assuming, for the sake of simplicity, the temporal variance of warm-sector temperature anomalies does not depend on latitude, then a decrease of the mean temperature towards the pole implies a reduction of the variance in specific humidity (at constant relative humidity). Thus, towards the pole the anomalies in specific humidity decrease relative to temperature anomalies and thereby the percentage to $v'm'_{\mathrm{TE}}$.

Six-hourly accumulated precipitation is overlaid in Fig. 5d-e with black contours. The signal is spatially prominent in the warm sector, yet its peak is spatially shifted by around $3°$ towards the cyclone center compared to the maximum in $v'Lq'_{\mathrm{TE}}$. From a moisture budget perspective, precipitation is balanced by evaporation, column moisture storage, and the convergence of latent heat flux. A large meridional transport of latent heat per se does not have to yield a large latent heat flux convergence, which in turn does not imply a release of latent heat (and related precipitation) because the converging specific humidity could — in principle — also be completely stored within the column. Indeed, the composite maxima of vertically integrated (eddy) latent heat flux convergence and precipitation do not align either (not shown).

This latitudinal separation highlights that cyclones at lower latitudes disproportionately influence the MSE flux signals in Figs. 3 and 4 especially due to the Clausius-Clapeyron relationship. Therefore, analyses involving aggregation of eddy MSE fluxes across wide ranges of latitudes (Figs. 3 and 4 or, e.g., Messori and Czaja, 2015) should be interpreted with care.

https://doi.org/10.5194/egusphere-2025-2314
Preprint. Discussion started: 30 May 2025

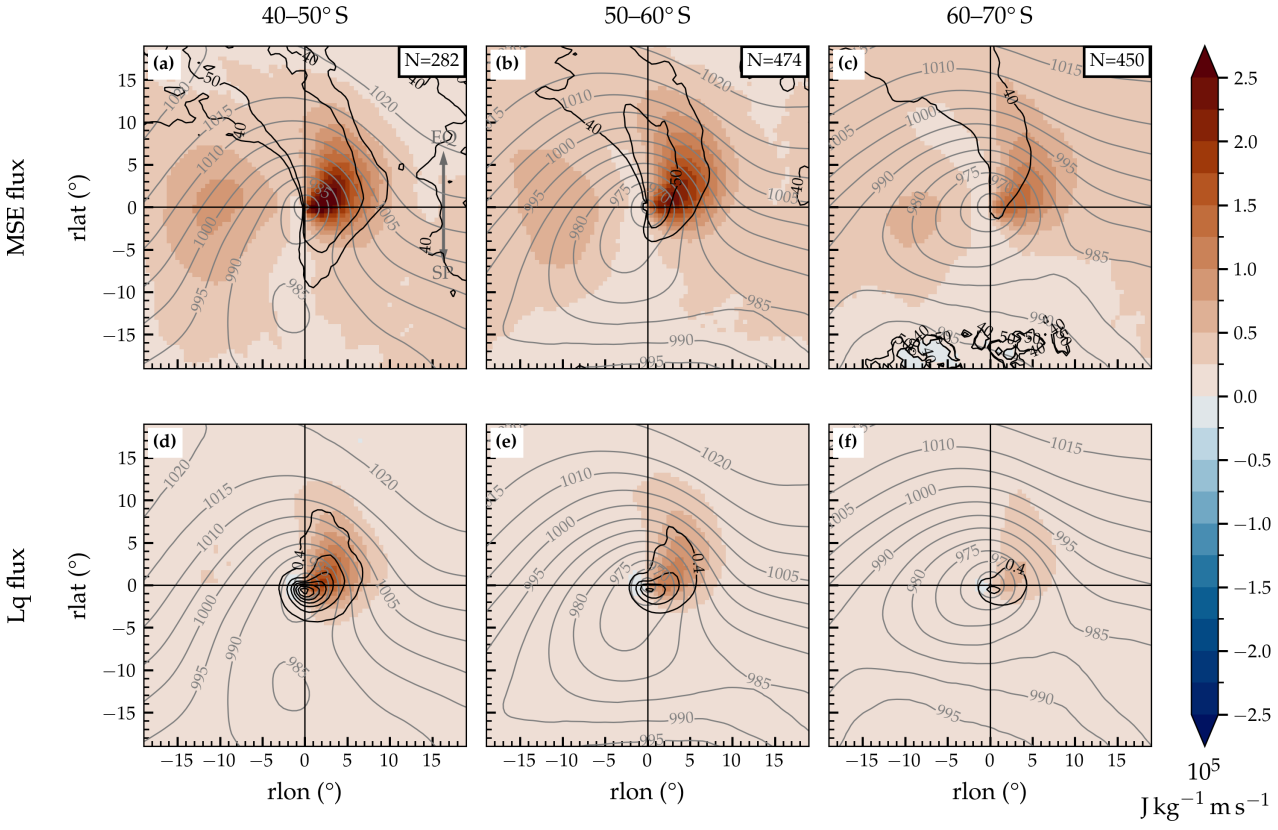

Figure 5. Cyclone-centered TE MSE flux, $v'm'_{\mathrm{TE}}$, at 850 hPa composited during time of peak intensification for cyclones with center within **(a)** 40–50° S, **(b)** 50–60° S, and **(c)** 60–70° S. As in **(a)–(c)**, the latent heat component, $v'Lq'_{\mathrm{TE}}$, is separately shown in panels **(d)–(f)** for the corresponding latitudinal ranges. Regions where latent heat flux makes up for 40 % and 50 % of the MSE flux are outlined with black contours in **(a)–(c)**. Black lines in **(d)–(f)** depict precipitation in steps of $0.4\,\mathrm{mm\,h^{-1}}$. Grey contours indicate composite mean SLP in hPa. The number of cyclones in the composites are included in the upper right in panels **(a)–(c)**. A grey arrow is included for better orientation indicating the directions of the equator (EQ) and South Pole (SP).

Overall, the cyclone-centered perspectives supports and complements previous findings on (low-level) eddy MSE flux extremes (Messori and Czaja, 2015; Geen et al., 2016; Messori et al., 2017). The following sections discuss vertically integrated TE MSE fluxes and discuss the influence of the cyclone characteristics on the zonally integrated AHT. As particular focus is on the intensification rate, it is worth pointing out that the previous findings regarding the horizontal structure of the eddy MSE fluxes around cyclones are also valid for vertically integrated fluxes and different flux decompositions (see Appendix C, Fig. C2).

https://doi.org/10.5194/egusphere-2025-2314
Preprint. Discussion started: 30 May 2025

4 How do different cyclones contribute to zonally integrated AHT?

It is known that an instantaneous zonal flux extreme is partly driven by the number and intensity of coexisting warm and cold sectors (Messori and Czaja, 2015). A few of these zonal flux extremes in turn have a disproportionate impact on the seasonal mean flux throughout the extratropics (Messori and Czaja, 2015). Having studied evolution of $v'm'_{\mathrm{TE}}$ along the cyclone life cycle, the results of the previous section suggest that the intensification rates of cyclones could play an important role in setting instantaneous and seasonal zonal mean energy flux. The goal of this section is to explore whether and and how different cyclone characteristics are reflected in the vertically and zonally integrated TE MSE flux, $\langle[v'm'_{\mathrm{TE}}]\rangle$.[3] For instance, are strongly intensifying cyclones related to higher $\langle[v'm'_{\mathrm{TE}}]\rangle$ than weakly intensifying ones? Answering such questions requires linking TE MSE flux to individual cyclones. Ideally, the chosen attribution method resolves the latitudinal shift between the maxima of cyclone frequency and eddy MSE flux, respectively (Fig. 1b). Thereby, the cyclone track and zonal energy budget perspectives would become better connected. Hereafter, vertically integrated flux data are used to simplify the task.

4.1 Attributing eddy fluxes to cyclones

How can $\langle v'm'_{\mathrm{TE}}\rangle$ be attributed to a cyclone? One simple approach is to use the SLP-derived cyclone masks (see Sect. 2.2) to label the instantaneous TE MSE flux fields. Using that approach, the TE MSE flux captured within the cyclone masks is broadly below than 1 PW (black dashed line in Fig. 6a) and barely reaches 30 % of the overall $\langle[\overline{v'm'}_{\mathrm{TE}}]\rangle$ (Fig. 6b).[4] The low fraction of TE MSE flux within the cyclone mask is consistent with the cyclone composites (e.g. Fig. 3b, c, Fig. 4a): A substantial fraction of the poleward flux does not occur in close vicinity to the cyclone center but further downstream and equatorward. In the composite, this partly lies outside of the lowest closed SLP contour which, for the sake of the argument, can be regarded as a proxy for the cyclone mask. Moreover, the correlation between seasonally averaged overall and cyclone-masked fluxes is low (and even negative) across the midlatitudes (black line in Fig. 6c) because very little of the overall TE MSE flux occurs within the cyclone mask.

To overcome issues related to the spatial displacement discussed above, eddy MSE flux features are identified and attributed to nearby cyclones based on spatial overlap (see Sect. 2.5 for more details). For each cyclone, the fluxes within these attributed features are retained and yield a zonally integrated cyclone-attributed TE MSE flux, $\langle[v'm'^{\mathrm{cycl}}_{\mathrm{TE}}]\rangle$, as sketched out in Fig. 7. Considering all cyclones within a season, the seasonal mean cyclone-attributed TE MSE flux thus reads $\langle[\overline{v'm'}^{\mathrm{cycl}}_{\mathrm{TE}}]\rangle$. Note that in the following, the overbar denotes the seasonal mean computed from monthly means whereas dashes still represent anomalies from monthly means as introduced in Sect. 2.3. Using this attribution method, the percentage of captured TE MSE flux is increased by 15–20 % (Fig. 6b) — relative to only counting TE MSE fluxes within the cyclone mask. Additionally, the correlation of seasonal means between the total cyclone attributed flux ranges from 0.5 around 40° S to 0.75 poleward of 55° S (dark orange line in Fig. 6c). A priori, one should not expect a 100 % flux coverage or perfect correlation due to the presence of other dynamical features such as anticyclones. Additionally, the cyclone attribution method improves the meridional offset

[3] In the result sections, we use square brackets for zonal means and integrals interchangeably.
[4] The percentage can surpass 100 % if fluxes outside of the cyclone masks are predominantly equatorward.

https://doi.org/10.5194/egusphere-2025-2314
Preprint. Discussion started: 30 May 2025

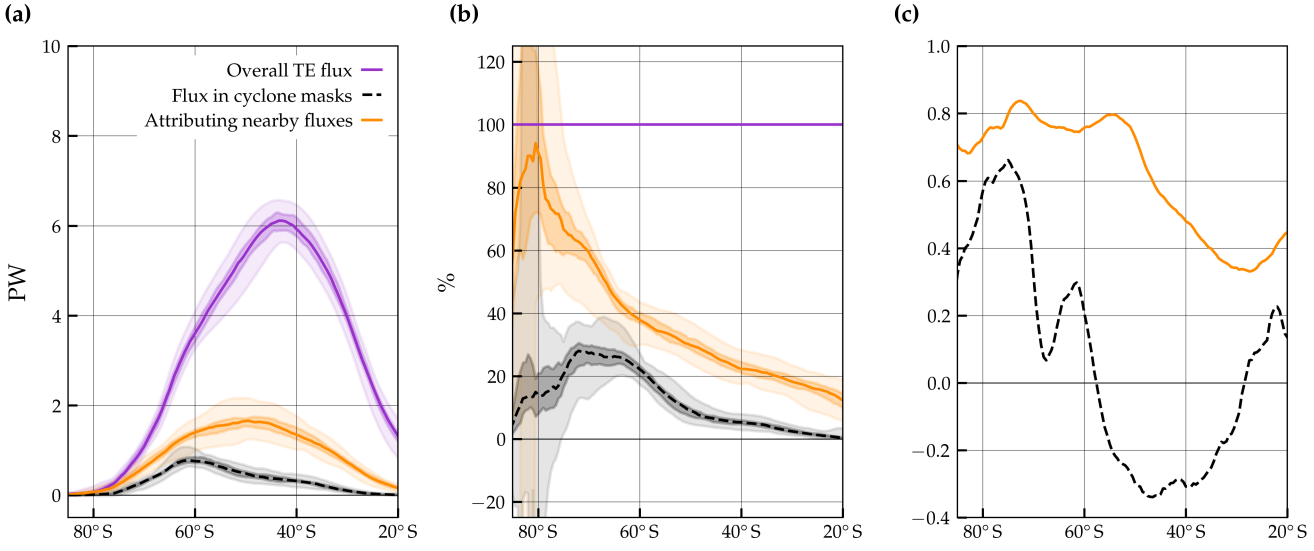

Figure 6. Seasonal TE MSE fluxes in SH winter: **(a)** the overall TE MSE fluxes, $\langle[\overline{v'm'}_{\mathrm{TE}}]\rangle$, shown in purple are contrasted to the TE MSE fluxes within cyclone masks (black, dashed) and the TE MSE fluxes within features that are attributed to cyclones, $\langle[\overline{v'm'}^{\mathrm{cycl}}_{\mathrm{TE}}]\rangle$ (dark orange). Solid and dashed lines indicate medians, light shading the full range, and darker shading the inter-quartile range of the seasonal means for the years considered. **(b)** As **(a)** but expressed as a percentage of the corresponding seasonally averaged overall TE MSE flux (which is 100 % by definition). **(c)** Correlations of seasonally averaged fluxes with overall TE MSE fluxes.

between the maxima in the overall and cyclone attributed flux. The maxima in the TE MSE flux within cyclone masks occurs around 20° poleward of the overall TE MSE flux $\langle[\overline{v'm'}_{\mathrm{TE}}]\rangle$. In contrast, the fluxes that are attributed to cyclones, $\langle[\overline{v'm'}^{\mathrm{cycl}}_{\mathrm{TE}}]\rangle$ (dark orange), peak around 10° further equatorward of the ones within the SLP masks and thus more closely to the peak of $\langle[\overline{v'm'}_{\mathrm{TE}}]\rangle$ (purple distribution in Fig. 6a). The remaining latitudinal discrepancy may partly arise due to the SLP-based tracking method not detecting cyclones further equatorward (Sinclair, 1994). Overall, with the composite results of Sect. 3.2 in mind the latitudinal shift of the zonally integrated flux (Fig. 6a) suggests that the attribution method is more useful for studying the effect of cyclones on zonally integrated AHT than simply the cyclone masks because adjacent warm and cold sectors are captured. Thereby, this method is a comprehensive solution to connect the surface cyclone and MSE flux frameworks.

4.2 Cyclone characteristics in the zonal integral

Attributing $\langle v'm'_{\mathrm{TE}}\rangle$ to individual cyclones allows for studying the influence of a cyclone characteristic on the zonally integrated transport. For the seasonal timescale, the accumulated flux along the lifetime is informative while the averaged flux per time step is more useful when studying instantaneous energy transport. Findings from Sect. 3 suggest that the duration and magnitude of cyclone intensification are important for both timescales.

https://doi.org/10.5194/egusphere-2025-2314
Preprint. Discussion started: 30 May 2025

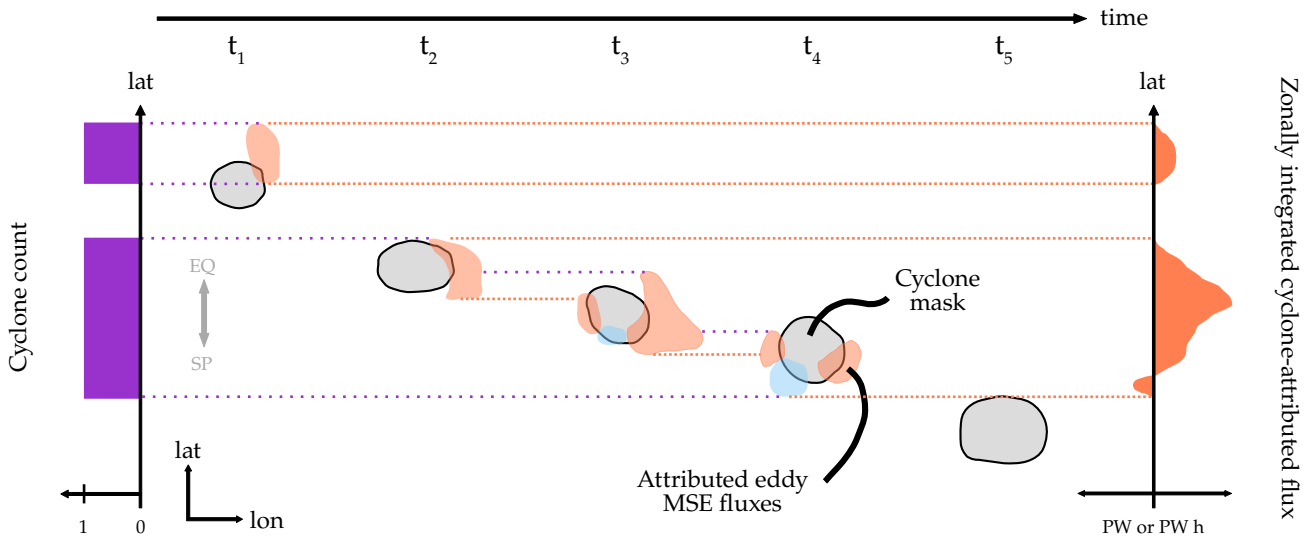

Figure 7. Schematic of the zonally integrated cyclone-attributed eddy MSE flux and the derived latitudinal extent, exemplified for a surface cyclone that lasts for five six-hourly time steps. The cyclone mask is indicated with grey patches and the attributed poleward and equatorward eddy MSE flux features with orange and blue shading, respectively. Cyclone-attributed eddy MSE fluxes are zonally integrated and are expressed in PW h if accumulated or in PW if averaged over the cyclone lifetime (orange curve). The latitudinal extent (or count) of this cyclone is then determined by the latitudes at which the attributed fluxes along its lifetime are non-zero. At any latitude band, a cyclone is therefore counted either once or zero times (purple bars). A grey arrow serves orientational purposes.

Accumulated over their lifetime, the 200 SH cyclones (Catto et al., 2010; Sinclair et al., 2020) that intensify most strongly are, on average, associated with poleward TE MSE transport of around 20 PW h at 50° S (blue solid line in Fig. 8a). In turn, the accumulated flux of the 200 cyclones with the lowest intensification rates amounts to only a few PW h around 65° S (red solid line in Fig. 8a). Given the large variability of cyclones, we advocate for interpreting these lines as the flux built up by many cyclones with a similar characteristic instead of a representation of 'the average cyclone' (see discussion in Sect. 4.3 below). In that sense, cyclones intensifying strongly accumulate 3–20 times the zonally integrated TE MSE flux of weakly intensifying cyclones (solid purple line in Fig. 8b). This difference is similar for the longest-lived cyclones (dashed line in Fig. 8b). Cyclone intensity emerges as an equally important differentiator for accumulated transport, although the fluxes are differently distributed across latitude (dotted lines in Fig. 8a). This can be explained by SLP climatologically decreasing towards the pole. The corresponding ratio in Fig. 8b (dotted line) is thus less informative.

Do strongly intensifying cyclones only transport more because they possibly exist longer? By dividing the accumulated flux by the cyclone lifetime, one obtains the averaged instantaneous flux. The averaged fluxes attributed to the most long- and short-lived cyclones become more comparable (dashed lines in Fig. 8c) which manifests in a ratio around 2 (Fig. 8d). In contrast, strongly intensifying cyclones retain much higher instantaneous flux compared to the weakly intensifying ones with the ratio

https://doi.org/10.5194/egusphere-2025-2314
Preprint. Discussion started: 30 May 2025

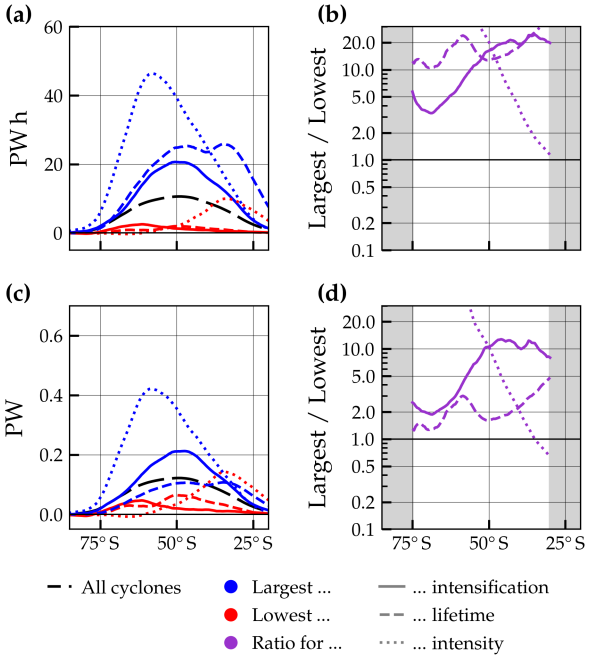

Figure 8. (a) Average zonally and vertically integrated TE MSE flux attributed to extratropical cyclones, $\langle [v'm'^{\mathrm{cycl}}_{\mathrm{TE}}] \rangle$, of similar characteristic. Instantaneous vertically integrated fluxes are integrated temporally over the lifetime of each cyclone and integrated longitudinally at each latitude. The accumulated flux is expressed in PW h which should allow for a comparison of instantaneous fluxes in PW and cyclone lifetimes in hours. For each characteristic, the flux of the 200 cyclones with the largest values of that characteristic is shown in blue and the lowest 200 ones in red, respectively. Solid, dashed, and dotted lines indicate intensification rate, lifetime, and intensity, respectively. For example, the least intense cyclones (which are the ones with the highest mature stage center SLP) are shown by the red dotted line. **(b)** Dividing the flux of the 200 largest cyclones by the flux of the 200 lowest cyclones yields the ratio for each characteristic with the same line-styles as in **(a)**. **(c, d)** As in **(a, b)**, respectively, but for the average flux per time step in PW. In panels **(a, c)**, the average fluxes computed from all SH JJA cyclones (from which the other subsets are chosen) are shown with black long dash lines. For latitudes where the absolute fluxes are consistently low, the ratio in panels **(b, d)** is masked out.

remaining between 2–12 depending on the latitude. Interestingly, the mean flux computed from all cyclones (black long-dashed line in Fig. 8c) is larger than of both longest and shortest cyclones. This could be explained by long-lived cyclones having a long weakening phase without large fluxes, while short systems are not the ones intensifying very strongly. In conclusion, the attributed fluxes are larger for strongly intensifying cyclones than for weakly intensifying ones not because they exist longer but because near-cyclone fluxes are larger at individual time steps.

The above analysis is repeated with the initial subset of cyclones intensifying within 50–60° S. This should provide a 'fairer' comparison of intense vs. weak cyclones in light of the poleward climatological SLP decrease. Furthermore, the minimum lifetime is set to three days to avoid comparing 30 h tracks to seven-day tracks. Overall, a very similar picture emerges as

https://doi.org/10.5194/egusphere-2025-2314
Preprint. Discussion started: 30 May 2025

compared to the analysis on all SH cyclones. Again, the most intense, most strongly intensifying, and the longest cyclones are linked to high accumulated $\langle [v'm'^{\mathrm{cycl}}_{\mathrm{TE}}] \rangle$ (Fig. 9a) with ratios between 4–20 within 50–60° S (Fig. 9b). Lifetime remains a smaller differentiator when considering the instantaneous timescale (Fig. 9c,d) than the other two characteristics.

Note that the intense cyclones are linked to a $\approx 50\,\%$ higher averaged flux than the strongly intensifying ones (blue dotted vs. solid lines in Fig. 9c). The previous composites (Fig. 4) indicate that the magnitude of the fluxes is similar during the intensification phase for these two sets of cyclones.[5] The difference can be at least partly explained by the deepest cyclones covering a roughly $20\,\%$ larger area than the most strongly intensifying ones, which agrees with the size of the cyclone being more tightly related to the intensity than to the intensification rate (Rudeva and Gulev, 2007). The larger size of the cyclone mask and a slightly larger areal extent of the warm-sector fluxes also manifest in the composites (although those are only snapshots of the full life cycle, Fig. 4a,c). Consequently, there is more cyclone-attributed flux located further downstream of the cyclone center (not shown). Using a constant radius to define cyclone masks and attribute fluxes would lead to differences solely due to variations of the spatial extent not being accounted for — *unjustly* when acknowledging the diversity of cyclones, or *purposefully* if one were to study the influence of mask size on the results. Repeating the above analyses for the cyclones of largest poleward propagation speed reveals lifetime-averaged fluxes comparable to those of the most intense cyclones at some latitudes (not shown). Yet, poleward propagation speed is not the characteristic for which the cyclone-attributed *eddy MSE* fluxes are consistently the largest. Previous research suggests that either this is different for *total moisture* flux or that more fluxes are attributed to rapidly poleward propagating cyclones (compared to others) when using a constant radius (Sinclair and Dacre, 2019).

To summarize, the intensification rate of cyclones does modulate both instantaneous and accumulated zonally integrated eddy MSE transports. Strongly intensifying cyclones, on average, transport more eddy MSE flux poleward than weakly intensifying ones. This matches with what one could conjecture from the previous cyclone life cycle results. Importantly, the fluxes attributed to intense cyclones are even larger on both time-scales than those of the strongly intensifying ones. This analysis thus shows that not only the intensification rate but also the spatial extent (related to the intensity) are important determinants of the energy footprint of a cyclone in the zonal picture. Before moving on to addressing how the number of such cyclones relates to (eddy) AHT on a seasonal scale, we present some important considerations on the adopted flux attribution approach. These influence how the role of the cyclone number for AHT is examined.

4.3 On the challenges of flux attribution and limits to its interpretation

The chaotic nature of the atmosphere can be seen as it featuring various kinds of eddies (e.g. Barnes and Hartmann, 2012). Likewise, but from a traditionally and methodologically complementary perspective, it can also be acknowledged by appreciating the various types of surface cyclones (e.g. Troup and Streten, 1972). In this light, attributing column-integrated eddy MSE flux to surface cyclones to improve our understanding of atmospheric dynamics might seem like a bold endeavor. We briefly discuss methodological sensitivities of the above results and put forward limits of their interpretability.

[5] Note that the sets of cyclones are not identical.

https://doi.org/10.5194/egusphere-2025-2314
Preprint. Discussion started: 30 May 2025

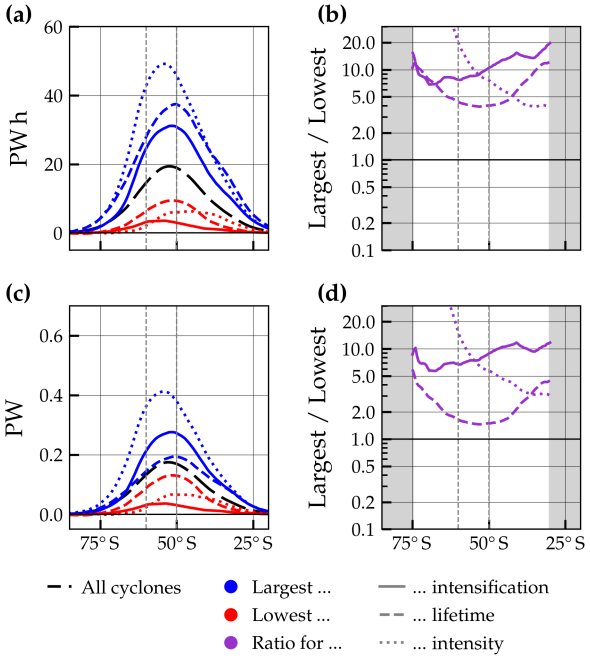

Figure 9. (a)–(d) As in Fig. 8 but restricted to the subset of cyclones which reach their peak intensification within 50–60° S (dashed vertical lines) and have a minimum lifetime of 3 days.

Individual cyclones can be associated with a lifetime-accumulated poleward energy flux beyond 100 PW h across a latitude band of the order of 10° (Fig. D1a). Additionally, the sample mean is much more extended in latitude than are individual events. This prompts the above framing that the averages depicted in Figs. 8 and 9 are not representative of individual cyclones. Instead, the above sample means are proposed to be interpreted as the accumulated fluxes due to several cyclones with similar characteristic.

Importantly, studying individual cyclones using these methods is not advisable because depending on the exact method the attributed fluxes can be vastly different for the same cyclone (Fig. B2). Firstly, changing the percentile used for identifying flux features affects their areal extent and therefore their overlap with cyclones. Secondly, different flux decompositions filter out different kinds of stationary flows. An instantaneous anomaly from the zonal mean (which is how eddy flux is defined in the ZA framework, see Sect. 2.3), for instance, might contribute to stationary eddy (and not transient eddy) flux in the TE framework if the anomaly is persistent enough. In this section, it is assumed that the biases arising from the two arguments average out for large enough cyclone numbers and in regions without systematic (climatological) temporal flow stationarity (≈ the SH midlatitudes). The influence of different decomposition methods is further addressed in Sect. 5.2.

Due to the relative simplicity of the attribution method, the sensitivity analysis of the above results boils down to 1) the choice of percentile for defining flux features and 2) the flux decomposition method. Qualitatively, the increase in attributed flux and increase in correlation (Fig. 6c) are robust to the choice of both percentile and flux decomposition method (Fig. D2).

https://doi.org/10.5194/egusphere-2025-2314
Preprint. Discussion started: 30 May 2025

Choosing lower percentiles moves the peak of the attributed fluxes towards the equator because larger masks (warm sectors extending further equatorward than the cyclone mask) are more often attached (Fig. D2a,d,g,j). The cause of the relatively reduced correlation around $60°$ S for the ZA framework (Fig. D2i) is not clear but might be related to the presence of planetary waves. A repetition with an upper integral bound of $500\,\mathrm{hPa}$ (Fig. D2l) suggests this signal arising from lower levels (and not stratospheric dynamics). Regarding the lifetime-averaged fluxes, the general conclusions on the roles of cyclone intensity, intensification rate, and lifetime remain valid for both cyclone samples (Figs. D3, and D4). Intensity and intensification rate consistently are more important differentiators than lifetime, albeit the ratio of lifetime varying between 1 and 2 (Figs. D5 and D6). Therefore, our discussion does not put emphasis on the exact factor of how much more eddy MSE flux is attributed to the largest versus lowest cyclones of each characteristic.

Lastly, when measuring the intensification rate in $\mathrm{Bergeron}$ instead of a simple finite SLP difference over time (Sanders and Gyakum, 1980), for all SH cyclones one observes a similar behavior as for the intensity: the more strongly intensifying cyclones (and their attributed fluxes) are located further equatorward than their counterparts (not shown). Within the more restrictive sample using the $10°$ latitude band, the attributed fluxes are slightly larger while the ratio is not substantially affected by the choice of intensification metric (not shown).

5 Linking seasonal cyclone characteristics and AHT

Finally, we investigate the relationship between extratropical cyclones and the zonally and vertically integrated TE MSE flux, $\langle [v'm'_{\mathrm{TE}}] \rangle$, on a seasonal scale. Given that large TE MSE fluxes can be attributed to strongly intensifying and intense cyclones, we examine how the seasonal number of these storms (or the overall cyclone number) relates to the seasonal mean zonally integrated eddy MSE flux and, ultimately, the total AHT. We focus on the latitude of $50°$ S which corresponds to the peak of the cyclone-attributed eddy MSE fluxes (Fig. 6a) and a correlation of around 0.7 between the attributed and the overall eddy MSE fluxes (Fig. 6c). The seasonally averaged TE MSE flux attributed to cyclones is denoted with $\langle [\overline{v'm'}^{\mathrm{cycl}}_{\mathrm{TE}}] \rangle$ as in Sect. 4. When addressing method dependencies, eddy fluxes derived from the other flux decompositions are denoted with the corresponding subscripts and dashing conventions (consistent with Sect. 2.3).

The seasonal number of cyclones is determined using the introduced flux attribution method: A cyclone is counted once towards all latitude bands where its attributed eddy MSE flux is different from zero along its lifetime (purple bars in Fig. 7). Thus, the seasonal number of cyclones at a given latitude corresponds to the cyclones that have attributed eddy MSE flux at this latitude, whereas their corresponding life cycle characteristics, such as maximum intensification rate or maximum intensity, can occur at any latitude. Based on this, the seasonal sub-sets of strongly intensifying and intense cyclones are determined using climatological thresholds: Cyclones are considered strongly intensifying if their intensification rate lies above the 75^{th} percentile determined from the climatological set of all cyclones passing that latitude. Note that the number of strongly intensifying cyclones for a given season is thus *not* simply $25\,\%$ of the overall cyclone number of that season. If the 75^{th} percentile of cyclone intensification based on all SH JJA cyclones is, for instance, $24\,\mathrm{hPa\,d^{-1}}$, the number of cyclones above this threshold in a season is not dependent on the corresponding number of all cyclones during that season. Choosing the

https://doi.org/10.5194/egusphere-2025-2314
Preprint. Discussion started: 30 May 2025

75th percentile instead of a higher one is a compromise between selecting only the strongest cyclones and including a large enough number of cyclones to counteract the event-to-event variability and method dependency discussed in Sect. 4.3. If the intensification rate lies within the inter-quartile range or below, cyclones are denoted moderately or weakly intensifying, respectively. The classification of cyclones as strong, moderate, and weak works analogously for intensity.

5.1 Seasonal eddy MSE fluxes and cyclone number

Strongly intensifying cyclones (above the climatological 75th percentile) account for roughly 43 % of $\langle[\overline{v'm'}^{\text{cycl}}_{\text{TE}}]\rangle$ at 50° S (yellow box in Fig. 10). This number is slightly higher for intense cyclones. For both intensity and intensification, the fluxes attributed to moderate cyclones (with the respective characteristic between the 25th and 75th percentiles) are of similar magnitude ($\approx 40-50\,\%$, grey boxes in Fig. 10). This is remarkable because this definition of moderate cyclones includes, on average, twice as many cyclones as the strong cyclones yet both categories are attributed a similar flux. Weak and weakly intensifying cyclones, in turn, only account for around 10 % of the attributed fluxes each season. Comparing the attributed fluxes of these groups of cyclones to the overall TE fluxes, the fractions reduce by a factor of three (not shown) in accordance with how much of overall eddy MSE flux is attributed to cyclones (Fig. 6b). Thus, intense (and strongly intensifying) cyclones disproportionately contribute to $\langle[\overline{v'm'}^{\text{cycl}}_{\text{TE}}]\rangle$. This is in line with the Eulerian perspective adopted in Messori and Czaja (2015) who found that daily zonal heat fluxes above the 95th percentile account for around 13 % of overall eddy MSE fluxes in SH winter. Yet, more than half of the seasonal $\langle[\overline{v'm'}^{\text{cycl}}_{\text{TE}}]\rangle$ is unrelated to the most intense (or most strongly intensifying) cyclones, which suggests that their number may not be tightly connected to the seasonal $\langle[\overline{v'm'}^{\text{cycl}}_{\text{TE}}]\rangle$ or, more generally, $\langle[\overline{v'm'}_{\text{TE}}]\rangle$.

Indeed, the seasonal zonally and vertically integrated TE MSE flux attributed to cyclones, $\langle[\overline{v'm'}^{\text{cycl}}_{\text{TE}}]\rangle$, is not highly correlated with either the number of strongly intensifying (n_{intensif}) or the number of intense (n_{intense}) cyclones. In other words, the number of intense or strongly intensifying cyclones does not determine (by itself) the TE MSE flux that is attributed to all cyclones during a season. Conversely, the correlation is higher with the overall cyclone number, n_{all} (Fig. 11a–c). When considering the overall TE MSE flux ($\langle[\overline{v'm'}_{\text{TE}}]\rangle$) instead, the relationship between the number of intense cyclones exhibits a larger correlation (Fig. 11f). The correlation with the overall cyclone number slightly decreases but is still visible in Fig. 11d. This implies that the attribution of TE MSE flux to cyclone masks reduces the link between the seasonal averaged attributed flux and intense cyclones (cf. Fig. 11c and f). While this suggests that on a seasonal scale $\langle[\overline{v'm'}^{\text{cycl}}_{\text{TE}}]\rangle \sim n_{\text{all}}$ and $\langle[\overline{v'm'}_{\text{TE}}]\rangle \sim n_{\text{intense}}$, these correlations vary substantially with flux attribution percentile and flux decomposition method in both cases (Fig. E1b,h). As described in Sect. 2.3, these analyses are also carried out defining eddy fluxes from high-pass filtered fields (HP) and, separately, from zonal anomalies (ZA). In general, the correlations discussed above depend more strongly on the flux decomposition method than on the flux attribution percentile. For the 90 % flux attribution percentile rank, the correlation $\rho\left(\langle[\overline{v'm'}^{\text{cycl}}_{\text{HP}}]\rangle, n_{\text{all}}\right) = 0.39$ while $\rho\left(\langle[\overline{v^*m^*}^{\text{cycl}}_{\text{ZA}}]\rangle, n_{\text{all}}\right) = 0.70$ (Fig. E1b). Similarly, for the overall eddy MSE fluxes $\rho\left(\langle[\overline{v'm'}_{\text{HP}}]\rangle, n_{\text{intense}}\right) \geq 0.65$, whereas $\rho\left(\langle[\overline{v^*m^*}_{\text{ZA}}]\rangle, n_{\text{intense}}\right) \leq 0.27$ (Fig. E1h). Note that measuring intensification rate in Bergeron and intensity based on SLP anomalies from a climatology instead does not yield a qualitatively different picture (not shown).

https://doi.org/10.5194/egusphere-2025-2314
Preprint. Discussion started: 30 May 2025

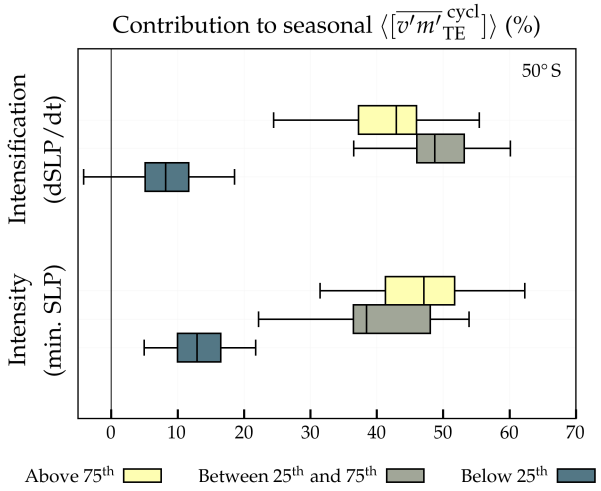

Figure 10. Percentage of seasonal TE MSE flux that is attributed to cyclones within three different ranges of intensification rate (top) and intensity (bottom). Percentages are shown in terms of cyclone-attributed TE MSE fluxes ($\langle[\overline{v'm'}^{\text{cycl}}_{\text{TE}}]\rangle$). Medians are shown with solid lines within the boxes, which in turn denote the interquartile range. Whiskers indicate 1.5 times the interquartile range while values outside of this range are not shown. MSE fluxes and cyclone numbers correspond to 50° S. For each life cycle characteristic, cyclones are grouped seasonally by the 25$^{\text{th}}$ and 75$^{\text{th}}$ percentiles derived from the climatological sets of cyclones that have non-zero $\langle[\overline{v'm'}^{\text{cycl}}_{\text{TE}}]\rangle$ at this latitude. The seasonal fluxes attributed to the cyclones that lie above the 75$^{\text{th}}$ percentile are represented in yellow, the ones between the 25$^{\text{th}}$ and 75$^{\text{th}}$ in grey, and the ones below the 25$^{\text{th}}$ in blue.

5.2 On method dependency

Given the large fraction of flux attributed to the cyclone sets of moderate intensity (or intensification, Fig. 10), it is not surprising to find low correlations with the number of intense (or strongly intensifying) cyclones. Previously, the main conclusions drawn in Sects. 3 and 4 based on large cyclone sample sizes were not sensitive to the flux decomposition method. Yet, as pointed out in Sect. 4.3 the fluxes attributed to individual cyclones can strongly differ from one method to the other. The high correlation between the number of intense cyclones and high-pass filtered eddy MSE flux — $\rho\left(\langle[\overline{v'm'}_{\text{HP}}]\rangle, n_{\text{intense}}\right)$ — relative to the weaker correlation between number of intense cyclone and MSE fluxes defined from zonal anomalies — $\rho\left(\langle[\overline{v'm'}_{\text{ZA}}]\rangle, n_{\text{intense}}\right)$ — is likely related to the contribution of stationary signals (in space or time) to the MSE flux and how these are treated in the MSE flux attribution method. In the frameworks tested in this study, a wave-like signal with a frequency $\sim (11\,\text{d})^{-1}$ is filtered out in the HP framework while it is partly attributed to cyclones in the ZA framework. While the choice of the cut-off frequency (or likewise the spatial wavenumber) can be motivated dynamically (e.g. Eady, 1949), some spectral power of a warm conveyor belt, for instance, is contained in the flow that is filtered out. Arguably, this is overestimated in the ZA framework which does not filter out *any* low-frequency waves. Yet, in a situation where a cyclone locally constructively interferes with a planetary wave it is only a subjective choice whether to attribute the entire or filtered energy flux to the cyclone, and the choice depends

https://doi.org/10.5194/egusphere-2025-2314
Preprint. Discussion started: 30 May 2025

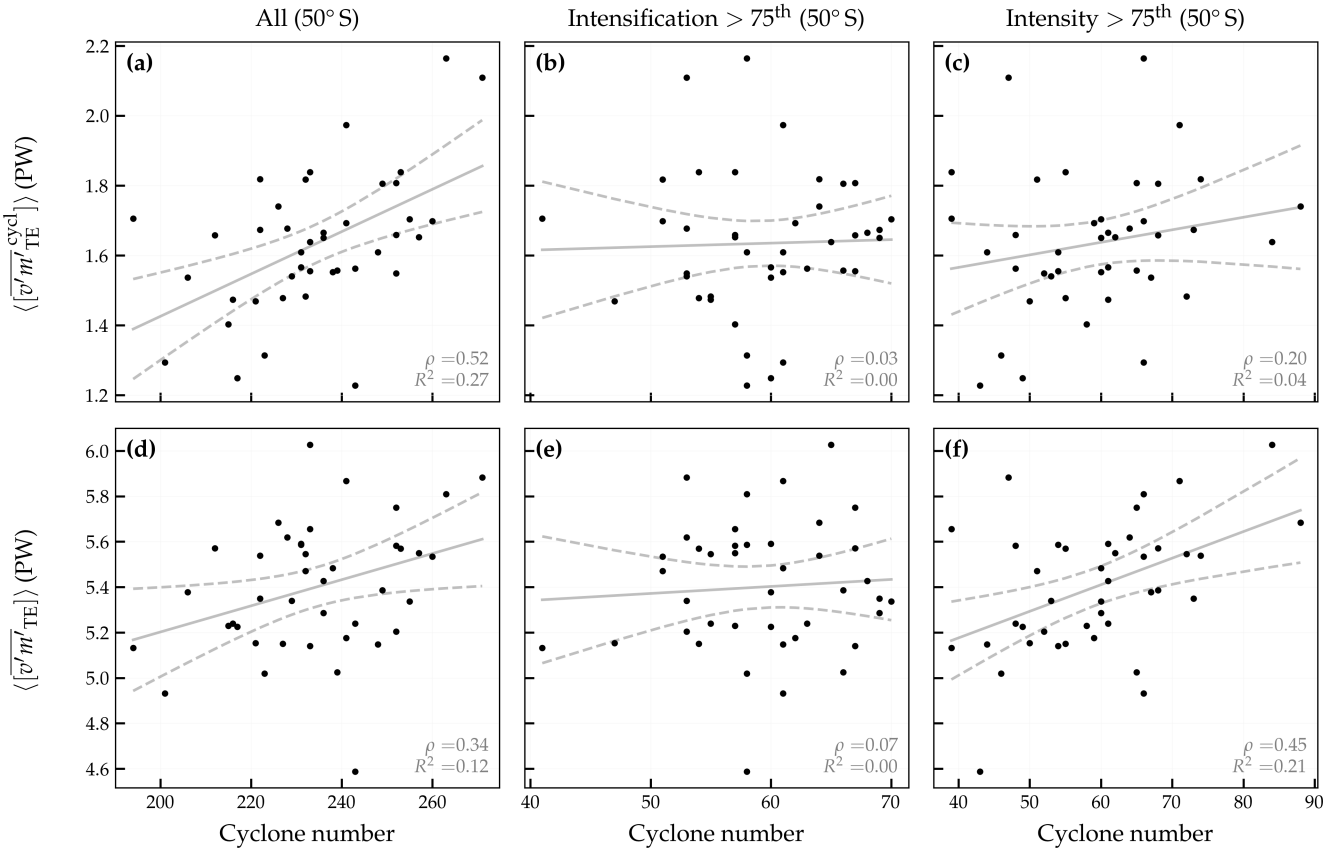

Figure 11. Relationship between seasonally averaged TE MSE flux and cyclone numbers for SH JJA at 50° S. **(a)** The cyclone-attributed TE MSE flux, $\langle[\overline{v'm'}^{\text{cycl}}_{\text{TE}}]\rangle$, in PW vs. the number of all cyclones with $\langle[\overline{v'm'}^{\text{cycl}}_{\text{TE}}]\rangle \neq 0$ at that latitude. **(b, c)** as **(a)** but for the number of strongly intensifying cyclones and intense cyclones, respectively. **(d)–(f)** as **(a)–(c)** but for the overall TE flux $\langle[\overline{v'm'}_{\text{TE}}]\rangle$. The grey solid line represents a best estimate of a linear fit and dashed grey lines the corresponding confidence band. Correlation (ρ) and explained variance of the linear fit (R^2) are indicated on the panels.

on the research question. $\rho\left(\langle[\overline{v'm'}_{\text{HP}}]\rangle, n_{\text{intense}}\right) > \rho\left(\langle[\overline{v^*m^*}_{\text{ZA}}]\rangle, n_{\text{intense}}\right)$ suggests that while the intensity of a cyclone has a footprint in the high-frequency flux component, the low-frequency waves that are attributed to it within the ZA framework convolve its energy footprint in the seasonal integral. The TE framework is a special case with the amount of background flows attributed to cyclones lying somewhere between the other two methods. Recall that in the TE framework, transient eddies are derived from monthly means whereas the monthly means give rise to stationary eddies (SE). All cyclones during the duration of a full month therefore may influence how much fluxes are attributed to an individual cyclone.

https://doi.org/10.5194/egusphere-2025-2314
Preprint. Discussion started: 30 May 2025

5.3 Cyclone numbers and total AHT

On the six-hourly timescale, eddy and overturning circulations are temporally anti-correlated in the midlatitudes (Cox et al., 2024b).[6] One could argue that the splitting into eddy and mean circulation of the flow is therefore not strictly related to circulation features (e.g., surface (anti-)cyclones, troughs, and ridges), which naturally contain signals from eddy and mean components because the mean was computed including the eddies in the first place. Thus, one would have to investigate the total AHT, $\langle[\overline{vm}]\rangle$ (the left-hand side of Eq. 2), instead of the eddy MSE flux. Recall, however, that the latitudinal extent of a cyclone and thereby the cyclone number were determined using the latitudinal extent of the *eddy* fluxes (Fig. 7). How can one obtain a cyclone number when addressing the *total* fluxes, which have not been locally attributed to cyclones so far, instead? One pragmatic way forward is to assume that the eddy MSE fluxes provide a good approximation of the latitudinal extent of the cyclone — i.e. continuing to count cyclones as above. Doing so yields a correlation between total AHT and cyclone number of $\rho(\langle[\overline{vm}]\rangle, n_{\text{all}})$ of 0.63 at $50°$ S for TE fluxes attributed with an attribution percentile rank of $90\,\%$. Note that this correlation remains dependent on the flux decomposition method and attribution percentile because those influence the latitudinal extent of the attributed fluxes and thereby the cyclone count (Fig. 7). Nevertheless, the dependency on the flux decomposition method (correlation between $0.40 - 0.64$, Fig. E1j) is comparably low. Of the latitude bands tested, however, $50°$ S is the latitude where this relationship is largest (Fig. E2j). The decrease towards the pole is not fully understood but in line with the relative importance of planetary-scale fluxes increasing towards the pole (Stoll et al., 2023). Notably, the correlations with n_{intense} and n_{intensif} are around zero throughout the SH (Fig. E1k, l). Note that taking the number of all cyclones in the entire SH, $n_{\text{all,SH}}$ (instead of the number of cyclones only at $50°$ S, n_{all}), the correlation reduces which suggests that capturing the latitudinal extent of cyclones is important ($\rho(\langle[\overline{vm}]\rangle, n_{\text{all}}) > \rho(\langle[\overline{vm}]\rangle, n_{\text{all,SH}})$, Fig. E1i,j).

To sum up, no robust relationship between the seasonal number of intense or strongly intensifying cyclones and the seasonal eddy MSE flux is identified. Conversely, total AHT at $50°$ S exhibits a correlation of $0.40 - 0.64$ with the number of cyclone passing that latitude during that season.

6 Summary and conclusions

6.1 Key findings

In this study we investigated the relationship between extratropical surface cyclones and AHT during SH winter (JJA) based on the ERA5 reanalysis. We connected these using (vertically and zonally integrated) eddy MSE flux and objectively identified cyclone tracks. The three central objectives of this study were to unveil the evolution of local meridional eddy MSE fluxes along the cyclone life cycles, to assess the footprint of a cyclone in the zonally integrated eddy MSE flux depending on its life cycle characteristics, and to explore the relationship between cyclone number and (eddy) AHT on the seasonal scale. In the following, the key findings are presented for each related research question in Sect. 1.

[6] In the TE framework, monthly mean TE fluxes are anti-correlated with SE+MOC fluxes

https://doi.org/10.5194/egusphere-2025-2314
Preprint. Discussion started: 30 May 2025

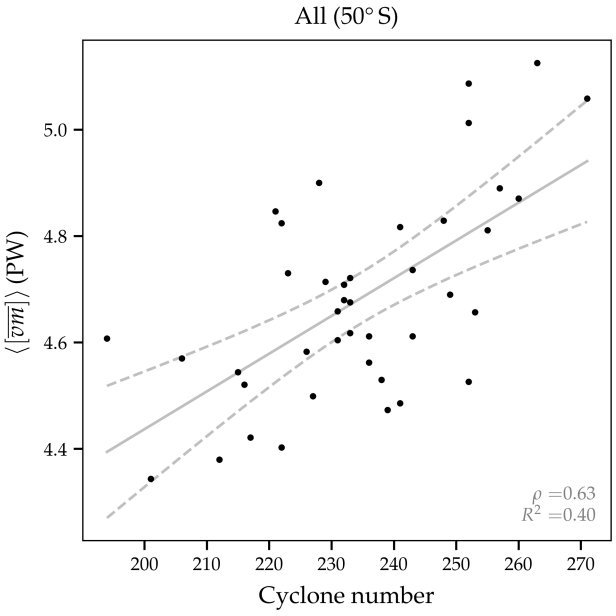

Figure 12. Relationship between seasonally averaged, zonally integrated total AHT, $\langle[\overline{vm}]\rangle$, in PW at 50° S and number of cyclones with a non-zero TE MSE flux attributed to them ($\langle[\overline{v'm'}^{\text{cycl}}_{\text{TE}}]\rangle \neq 0$) at the same latitude. Grey solid and dashed lines as in Fig. 11. Correlation (ρ) and explained variance of the linear fit (R^2) are indicated on the panel.

– Locally, meridional eddy MSE fluxes in the vicinity of cyclones peak during the intensification phase and before reaching mature stage (Fig. 2). Spatial composites reveal large fluxes in the warm sector confined by warm and cold fronts with a smaller signal in the cold sector (Fig. 3). Fluxes are enhanced for strongly intensifying and intense cyclones (Fig. 4). Crucially, a non-negligible fraction of warm-sector and cold-sector fluxes are located outside of the cyclone masks defined by closed SLP contours. Investigating the energy footprint of cyclones therefore requires attributing these fluxes to the cyclones as well. Doing so in our study increases the fraction of poleward eddy MSE flux attributed to cyclones and reduces the meridional offset between the maxima in cyclone mask frequency (and the fluxes therein) and the overall eddy flux (Fig. 6). This supports the notion that MSE fluxes within warm conveyor belts are important contributors to zonally integrated (eddy) heat transport proposed in Messori and Czaja (2015). With our approach, around 30 % of the overall (high-frequency or transient) eddy MSE fluxes are attributed to cyclones in midlatitudes.

– Considering the zonal integral, it was found that the life cycle characteristics influence the magnitude of cyclone-attributed eddy MSE fluxes. In particular, cyclone intensity is the life cycle characteristic for which the fluxes attributed to the strongest cyclones is largest (Fig. 9). Like intensity, the intensification rate also shows a large ratio of fluxes attributed to strong vs. weak cyclones. Poleward propagation speed, which is not discussed in detail, features a comparably large ratio at some latitudes but does not stand out over intensity (Sinclair and Dacre, 2019). The accumulated fluxes

https://doi.org/10.5194/egusphere-2025-2314
Preprint. Discussion started: 30 May 2025

increase with cyclone lifetime — naturally — but when normalizing by the number of time steps this characteristic is a much weaker indicator for the attributed flux.

– The previously identified link between cyclone intensity and attributed eddy MSE fluxes on the scale of individual cyclones also extends to the seasonal scale. Storms that have an intensity larger than the 75$^{\text{th}}$ climatological percentile collectively contribute to around 45 % of the seasonally integrated cyclone-attributed AHT (Fig. 10). This contribution is almost matched by the cyclones intensifying most strongly. For those two characteristics, the 'strong' cyclones thereby transport roughly as much eddy MSE flux as the 'moderate' cyclones despite the latter being, on average, twice as numerous. However, the fractions associated with the intense cyclones are not disproportionate enough for the number of these cyclones to be robustly linked to the seasonal eddy MSE flux (Fig. 11). This is further discussed below.

The approximate contributions of extratropical cyclones to the total AHT are summarized in Fig. 13: Cyclones contribute to the high-frequency (or transient) eddy AHT which, depending on the flux decomposition, is accompanied by low-frequency (or stationary) background fluxes and the mean overturning circulation. The high-frequency eddy MSE fluxes attributed to cyclones can be linked to different subsets of cyclones based on their intensity or intensification rate. Other high-frequency eddy MSE fluxes not attributed to cyclones may occur far from the cyclone center, be linked to high pressure systems, or be unrelated to weather features with closed contours such as meandering zonal flows.

6.2 The interplay of scales

Note that we broadly refer to high-frequency 'eddy' MSE fluxes in the above summary (instead of 'transient eddy' MSE fluxes specifically as in Sects. 3–5) since these conclusions overall do not depend on the choice of eddy-mean decomposition method. A consequential method dependence was only found for the correlation between the seasonal cyclone number and the eddy MSE flux (Fig. E1). This points to a non-negligible influence of planetary, low-frequency waves to the local eddy MSE flux attributed to individual systems (Messori and Czaja, 2014; Stoll et al., 2023). In other words, our results suggest that the influence of a cyclone characteristic on its energy footprint in the zonal integral is partly masked by a background signal of which a fraction is attributed to the cyclone. While for large enough sample sizes, this method-dependency averages out ($N \gtrapprox 200$ as in Sects. 3 and 4), this effect is thought to influence the picture when considering a seasonal set of intense cyclones, for instance ($N \approx 60$, Sect. 5). Recall that the most intense cyclones account for approximately half the cyclone-attributed eddy MSE flux. Therefore, under the somewhat naive assumption that cyclone-attributed eddy MSE fluxes were unrelated to background signals, one might have expected a correlation between the number of intense cyclones and the cyclone-attributed eddy MSE flux (Fig. 11f). Of the methods tested, high-pass filtering is most effective at separating synoptic signals and background flows — correspondingly, the correlation between eddy MSE fluxes and the number of intense cyclones is largest for this method. With more and more background fluxes being attributed to the cyclones when defining eddies from anomalies of monthly means, or instantaneously as anomalies from zonal means, the correlation decreases towards zero. At the same time, high-pass filtering is the method with the smallest fraction of total AHT explained by high-frequency eddies (Fig. D2).

https://doi.org/10.5194/egusphere-2025-2314
Preprint. Discussion started: 30 May 2025

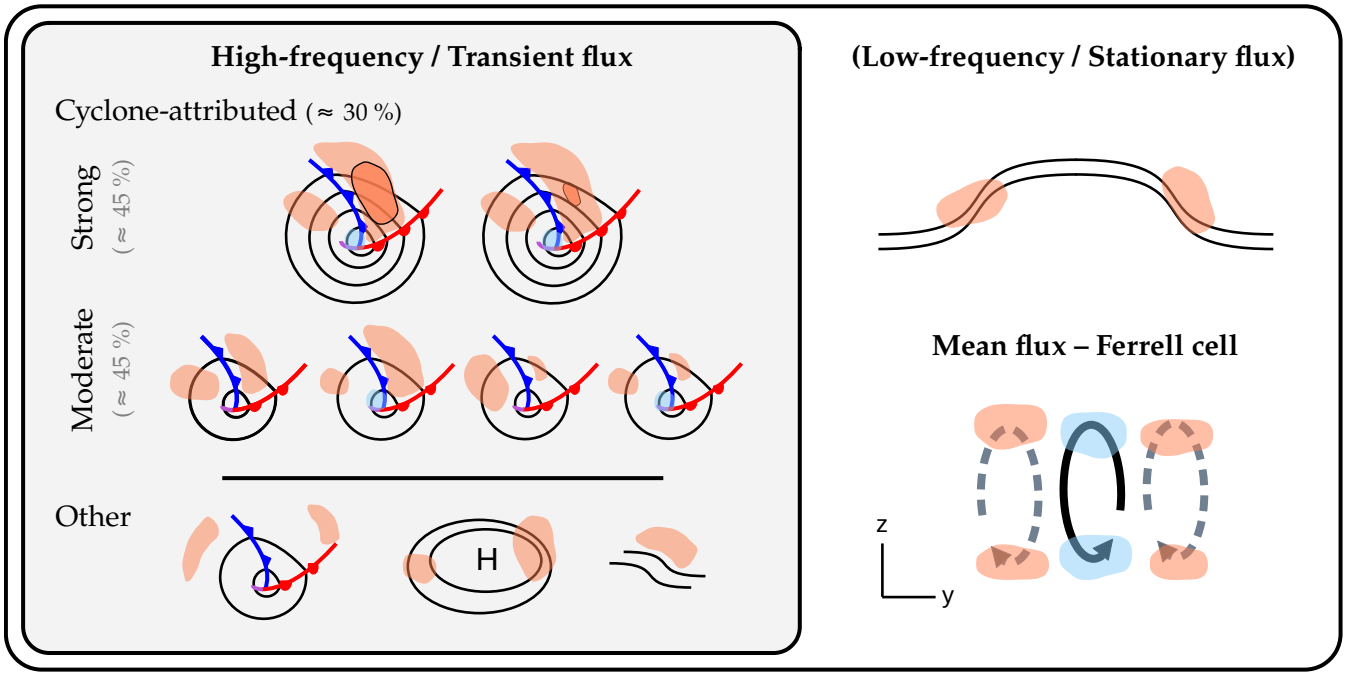

Figure 13. Schematic of the decomposition of total AHT into different flux components and contributions by extratropical cyclones: When adopting an eddy-mean decomposition, the AHT is the sum of a high-frequency, transient eddy flux component, potentially a separate low-frequency or stationary eddy component, and the zonal mean flux related to overturning. Orange and blue shading denotes poleward and equatorward meridional MSE fluxes, respectively. The high-frequency, transient eddy fluxes are further split into cyclone-attributed (≈ 30 % of the high-frequency eddy fluxes) and other fluxes. Surface cyclones in the left box are illustrated by SLP contours that are accompanied by warm fronts (red lines), cold fronts (blue), and occlusions (purple). 'Strong' and 'moderate' refer to the intensity or intensification rate of cyclones with 'weak' cyclones omitted. Grey percentage indications refer to the approximate contribution of those cyclones to the cyclone-attributed eddy MSE flux (and not the overall high-frequency eddy flux). Low-frequency or stationary flow is sketched by wave-like black lines in the top right. In the bottom right, the zonal mean flux is drawn in a latitudinal and vertical y-z cross-section with the overturning circulation illustrated with solid black (Ferrell cell) and dashed grey (Hadley and polar cells) arrows.

The lack of a robust relationship between seasonal cyclone numbers and seasonal mean eddy MSE flux suggests that the former is not directly constrained by planetary energetics. One can argue that this should not have been expected, however, because any energetic constraint would relate to the *total* AHT instead of the *eddy* AHT. Given an anti-correlation between eddy and zonal mean fluxes (Cox et al., 2024b), cyclones may be related to an arbitrarily large eddy flux which — compensated by the mean overturning — still fulfills the Earth's energy imbalance (Eq. 1). In addition to high-frequency (or transient) eddies, low-frequency (or stationary) eddies add further complexity depending on the decomposition method (Fig. 13). As the spectrum of total AHT is predominantly continuous (see for instance supplementary of Stoll et al., 2023), choosing a scale separation in time or space is a balance between how much low wavenumber flux is attributed to a background component — which poses a degree of freedom in AHT variability — and how it imprints in the eddy component, eventually near individual cyclones.

https://doi.org/10.5194/egusphere-2025-2314
Preprint. Discussion started: 30 May 2025

Conversely, abandoning a flow decomposition would require the definition of an atmospheric reference state such that cold air moving equatorward is identified as counteracting the equator-to-pole energy imbalance. Thus far, when inspecting the total AHT at $50°$ S we find that its correlation with the number of cyclones (counting those that contribute to the eddy AHT at that latitude) lies between 0.40–0.64 (Figs. 12 and E1j). The comparably high correlation is reduced at other latitudes (Fig. E2j), however, such that further research is needed to better understand whether changes in cyclone numbers can be related to AHT changes constrained by the Earth's energy imbalance.

6.3 Further remarks

Note that the contribution of low-frequency and planetary-scale waves to the zonally integrated AHT likely increases with height (Stoll et al. (as suggested by the dry and latent heat flux decomposition in 2023). Focusing on surface cyclones, one possible extension of this work is a repetition of the above analyses using only low-level fluxes. In addition to reducing the above sensitivity with respect to the definition of what is background flux, this would also segregate stratospheric contributions unrelated to surface weather. In the SH, we do not expect a strong influence of stratospheric fluxes on our results; at $65°$ S, stratospheric fluxes account for only $11\,\%$ of the column-integrated fluxes explaining $10\,\%$ of its variance (Cardinale et al., 2021).

While our analysis focused on SH winter, technically, the methods can readily be applied to the NH and other seasons as well. Yet, in the NH the stationary signal is much larger, which increases the sensitivity with respect to the flux decomposition method (not shown) and weakens the connection between AHT by cyclones and hemispheric scale radiative budget constraints. Furthermore, one has to reflect on whether and how to disentangle the signals arising from the Atlantic and Pacific basins due to different changes in cyclone characteristics. The response of the cyclone number to warming and storm track latitude, for instance, is different in these two basins (e.g. Seiler and Zwiers, 2016; Chang, 2018). Moreover, stratospheric contributions to the vertical integral are larger in the NH (Cardinale et al., 2021) such that one should consider a sensitivity analysis with respect to the vertical integration bound. Lastly, by neglecting zonal heat fluxes we implicitly assumed that the energy imbalance is counteracted by heat being transported into a zonally symmetric polar cap. The larger zonal asymmetries in the NH (and horizontal tilting of storm tracks, Fig. 1a) question the applicability of this assumption as meridional heat fluxes alone might not accurately describe the circulation that underlies a possible energetic constraint.

More sophisticated methods for attributing different kinds of fluxes to cyclones (e.g., Fearon et al., 2021; Lopez-Marti et al., 2025) are conceivable. Warm and cold sector MSE fluxes could be identified using atmospheric river (Shields et al., 2018) or warm conveyor belt masks (Heitmann et al., 2024) and cold sector masks (Zolina and Gulev, 2003; Kolstad and Bracegirdle, 2008; Vannière et al., 2016), respectively. Note that depending on the identification method, WCB masks might require computing Lagrangian air parcel trajectories (Heitmann et al., 2024). Attributing fluxes via surface fronts is another possibility (Papritz et al., 2014), although it is unclear how well these capture fluxes throughout the sectors (Messori et al., 2017). Instead of attributing fluxes to cyclones, one could directly study the influence of warm conveyor belt and cold sector numbers on the zonal energy budget. Since fluxes do not peak near the center of weather systems but rather between cyclones

https://doi.org/10.5194/egusphere-2025-2314
Preprint. Discussion started: 30 May 2025

and anticyclones, that would make the question "What about the anticyclones?" — which we have dismissed so far — obsolete (Ruggieri et al., 2020).

This study has not addressed trends in either MSE fluxes or cyclone numbers. The introduced decrease of SH winter cyclones in a warmer climate, however, motivates further research on the relationship between extratropical cyclones and zonal mean energetics. A follow-up study is planned applying our diagnostics to aquaplanet simulations and future climate projections.

Code and data availability. The underlying ERA5 reanalysis data can be downloaded from https://doi.org/10.24381/cds.bd0915c6 (Hersbach et al., 2020). A code repository to reproduce the data and the figures and a data archive are in preparation and will be made accessible upon publication.

Appendix A: Abbreviations and terminology

To facilitate the lecture of this study, a list of abbreviations (Table A1) and frequently used mathematical terms (Table A2) is provided.

Appendix B: MSE flux attribution to cyclones and cyclone counting

In our study, we identify events of large eddy MSE fluxes based on a seasonally and latitudinally varying flux threshold. This threshold is computed by aggregating all values of a latitude band of the same time of every year and computing a percentile based on that distribution. This is illustrated in Fig. B1. The identified features are then attributed to surface cyclones using SLP-derived masks as shown in Fig. B2. Note that not all flux features overlap with cyclone masks (yellow patches in Fig. B2g–i).

Appendix C: Sensitivity and variability of near-cyclone eddy MSE fluxes

To further strengthen the conclusions drawn from the cyclone composites, a significance test is performed for the TE framework. For this we address the standardized flux anomalies (SFA) from the climatological seasonal mean, $v'm'^{\text{clim}}_{\text{TE}}$, defined as

$$\text{SFA}(lon, lat, time, pressure) = \frac{v'm'_{\text{TE}}(lon, lat, time, pressure) - v'm'^{\text{clim}}_{\text{TE}}(lon, lat, pressure)}{\sigma(v'm'_{\text{TE}})(lon, lat, pressure)} \tag{C1}$$

with σ the standard deviation over the climatological period. Locations in the composite where mean(SFA) $= 0$, we regard the $v'm'_{\text{TE}}$ of the individual events that we used for compositing as not significantly different from climatological $v'm'_{\text{TE}}$ fluxes. In other words, the null hypothesis, mean(SFA) $= 0$, is rejected if within the composite, fluxes are sampled that are on average different from climatology. We perform a two-sided, one sample *t*-test at each composite grid-cell (Fig. C1). Overall,

https://doi.org/10.5194/egusphere-2025-2314
Preprint. Discussion started: 30 May 2025

Table A1. List of abbreviations used in this study.

Abbreviation	Meaning
AHT	Atmospheric heat transport
DJF	December, January, February
EQ	Equator
HP	High-pass (filtering method, framework)
JJA	June, July, August
(r)lat	(rotated) latitude
(r)lon	(rotated) longitude
MOC	Meridional overturning circulation
MSE	Moist static energy
NH	Northern Hemisphere
SE	Stationary eddy
SFA	Standardized flux anomalies
SH	Southern Hemisphere
SLP	Sea level pressure
SP	South Pole
TE	Transient eddy (framework)
TOA	Top of atmosphere
WCB	Warm conveyor belt
ZA	Zonal anomaly (framework)

the dynamical features that were identified in the composites are based on flux anomalies that on average are significantly different from zero. Note that low $v'm'_{\mathrm{TE}}$ can be significant in the composite as it is lower than climatology.

Compared to the TE framework (see Sect. 2.3 for a description of the different frameworks), is also the intensification phase (and not the mature stage) during which fluxes are largest when adopting the HP and ZA decompositions (not shown). A comparison of the fluxes at peak cyclone intensification reveals that at $850\,\mathrm{hPa}$, high-pass filtered fluxes are marginally lower than TE fluxes (Fig. C2a,b). Moreover, the contrast between warm and cold sectors is reduced in the ZA framework (Fig. C2c), which could be explained by strong warm sector anomalies raising the instantaneous zonal mean MSE such that cold sector anomalies become larger compared to the other methods. Note that for the NH, the differences between TE and ZA are more pronounced (not shown) due to the time-stationary signal being declared as SE flux (Eq. 2). These descriptions are also valid for vertically integrated fluxes (Fig. C2d–f).

https://doi.org/10.5194/egusphere-2025-2314
Preprint. Discussion started: 30 May 2025

Table A2. Description of selected terms used in this study. Subscripts of eddy fluxes change in accordance with dashes and asterisks.

Term	Description
$v'm'_{\mathrm{TE}}$	Meridional eddy MSE fluxes derived from monthly anomalies
$v'Lq'_{\mathrm{TE}}$	Meridional eddy moisture fluxes derived from monthly anomalies
$v'm'_{\mathrm{HP}}$	Meridional eddy MSE fluxes derived from high-pass filtering
$v^*m^*_{\mathrm{ZA}}$	Meridional eddy MSE fluxes derived from instantaneous anomalies from the zonal mean
$[v'm'_{\mathrm{TE}}]$	Zonal mean (or zonally integrated) TE MSE fluxes
$\overline{v'm'}^{\,\mathrm{TE}}$	Monthly or seasonal mean TE MSE fluxes
$\langle v'm'_{\mathrm{TE}}\rangle$	Vertically integrated TE MSE fluxes
$\langle [v'm'_{\mathrm{TE}}]\rangle$	Vertically integrated zonal mean (or zonally integrated) TE MSE fluxes
$\langle [\overline{v'm'}^{\,\mathrm{TE}}]\rangle$	Seasonal mean zonally and vertically integrated ('overall') TE MSE fluxes
$\langle v'm'^{\mathrm{cycl}}_{\mathrm{TE}}\rangle$	Vertically integrated TE MSE fluxes attributed to cyclones
$\langle [v'm'^{\mathrm{cycl}}_{\mathrm{TE}}]\rangle$	Zonal integral of vertically integrated TE MSE fluxes attributed to cyclones
$\langle [\overline{v'm'}^{\mathrm{cycl}}_{\mathrm{TE}}]\rangle$	Seasonal mean zonal integral of vertically integrated TE MSE fluxes attributed to cyclones
$\langle [\overline{vm}]\rangle$	Seasonal mean ('total') AHT
$v'm'^{\mathrm{clim}}_{\mathrm{TE}}$	Climatology of meridional TE MSE fluxes
$\langle [\overline{v'^{,*}m'^{,*}}_{\_\_}]\rangle$	Seasonal mean zonal and vertical integral of 'overall' eddy MSE fluxes for an arbitrary framework
$\langle [\overline{v'^{,*}m'^{,*}}^{\mathrm{cycl}}_{\_\_}]\rangle$	Seasonal mean zonal integral of vertically integrated eddy MSE fluxes attributed to cyclones for an arbitrary framework
n_{all}	Seasonal number of cyclones with non-zero cyclone-attributed eddy MSE flux at latitude of interest
$n_{\mathrm{all,SH}}$	Seasonal number of cyclones within the entire SH

Appendix D: Method dependence of cyclone-attributed zonally integrated eddy MSE flux

As discussed in Sect. 4.3, a method sensitivity of the results in Sect. 4 based on attributing eddy MSE fluxes to cyclones is performed. Cyclone-attributed eddy MSE fluxes are shown for individual cyclones in Fig, D1 for the TE framework, in particular the cyclones that intensify least and most rapidly across the SH.

The seasonal contributions to eddy MSE flux by cyclones are shown in Fig. D2. For the ZA framework, the sensitivity is performed for vertical integrals from $\overline{p_S}$ to the TOA (Fig. D2g–i) and $\overline{p_S}$ to $500\,\mathrm{hPa}$ (Fig. D2j–l).

Regarding the method dependency of the zonally integrated eddy MSE fluxes attributed to cyclones of different life cycle characteristics, the lifetime-averaged fluxes of panels Figs. 8c and 9c are repeated in Figs. D3 and D4, respectively. The corresponding ratios are shown for lifetime-accumulated and lifetime-averaged fluxes in Figs. D5 and D6.

Appendix E: Sensitivity of the number–flux relationship to choice of flux decomposition method

While the relationships between different seasonal TE MSE fluxes and cyclone numbers are shown by scatter-plots (Fig. 11), for conciseness we only show the correlations for the different flux decompositions and attribution percentiles. In addition to

https://doi.org/10.5194/egusphere-2025-2314
Preprint. Discussion started: 30 May 2025

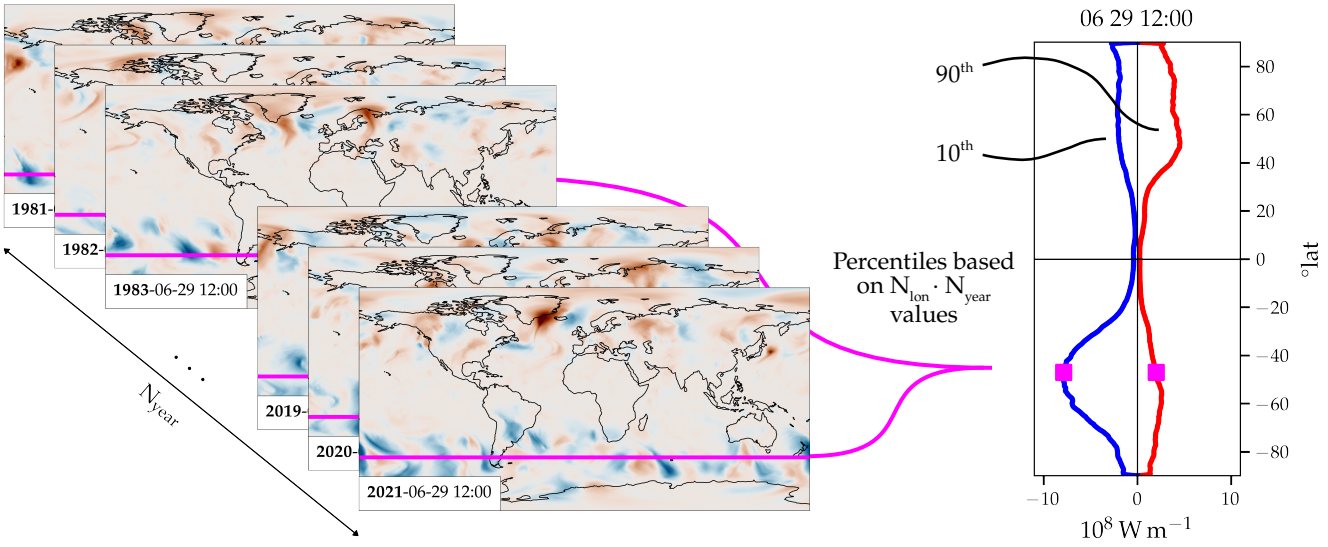

Figure B1. Illustration of the determination of the percentile threshold for eddy MSE flux events: For every six-hourly time step of a year — 29 June, 12:00 UTC, for instance — eddy MSE flux thresholds for poleward and equatorward fluxes are calculated at each latitude. These are based on the values of that latitude band and every corresponding time of year during the analysis period. Thus, the sample size which the percentile is computed from is the number of years (N_{lon}) times the number of grid-cells at a latitude circle (N_{lon}). The 10th and 90th percentiles of the vertically integrated eddy MSE fluxes (color shading on the left panel) for 29 June, 12:00 UTC are shown on the right in blue and red, respectively. The latitude of 47° S is highlighted in magenta.

the relationships discussed in Fig. 11, we show correlations with the number of cyclones in the entire SH ($n_{\text{all,SH}}$) and with total AHT ($\langle[\overline{vm}]\rangle$) — for 50° S in Fig. E1 and different latitudes in Fig. E2.

https://doi.org/10.5194/egusphere-2025-2314
Preprint. Discussion started: 30 May 2025

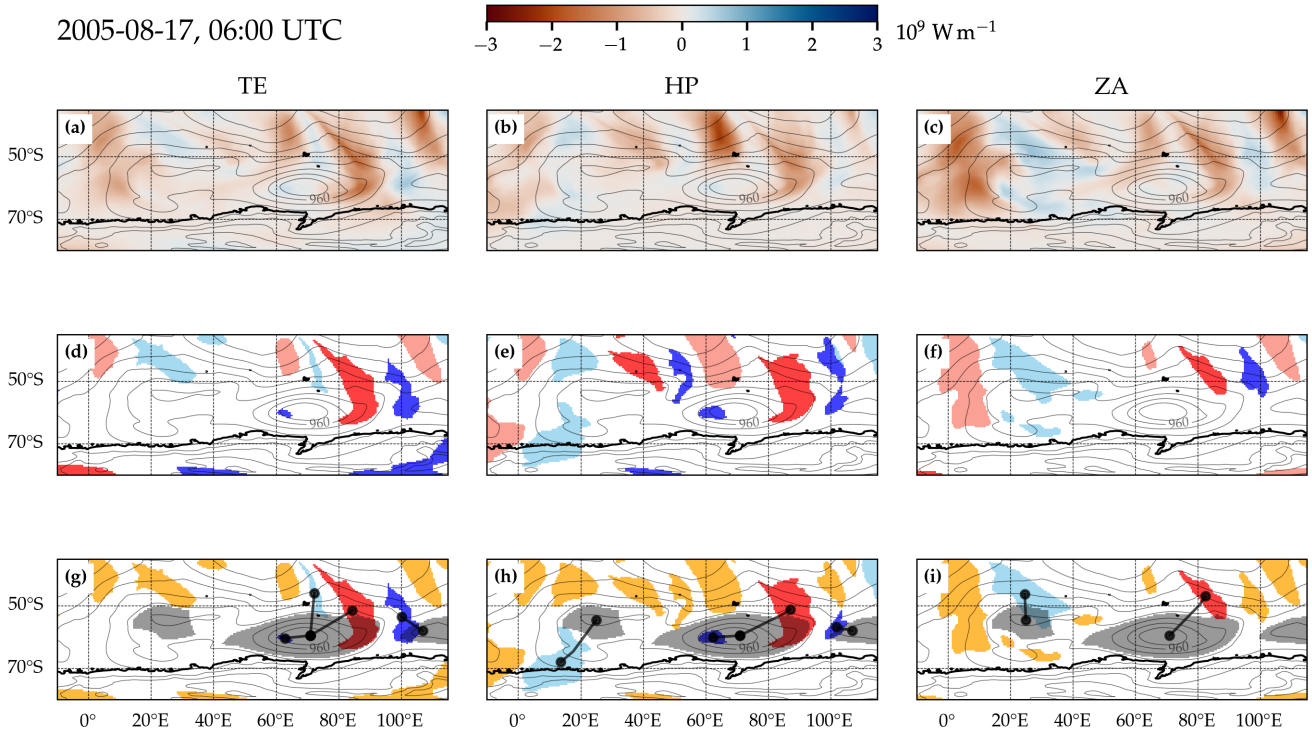

Figure B2. Snapshot of vertically integrated eddy MSE fluxes and their attribution to surface cyclones. **(a)** Vertically integrated eddy MSE fluxes calculated using the TE framework (shading in W m^{-1}) and SLP (black contours in steps of 10 hPa). **(b) and (c)** as in **(a)** but for the HP and ZA frameworks, respectively. **(d)–(f)** The binary masks corresponding to the identified flux features shaded in reddish and bluish colors if MSE fluxes are poleward or equatorward, respectively, and in dark and light tones if fluxes correspond to positive and negative MSE anomalies, respectively. **(g)–(i)** An addition to above, surface cyclone masks are shown with grey patches. If flux features are not overlapping with cyclones, the features are colored yellow. Otherwise, black straight lines and dots indicate to which cyclones the features are attributed to. Coastlines are depicted with black lines.

https://doi.org/10.5194/egusphere-2025-2314
Preprint. Discussion started: 30 May 2025

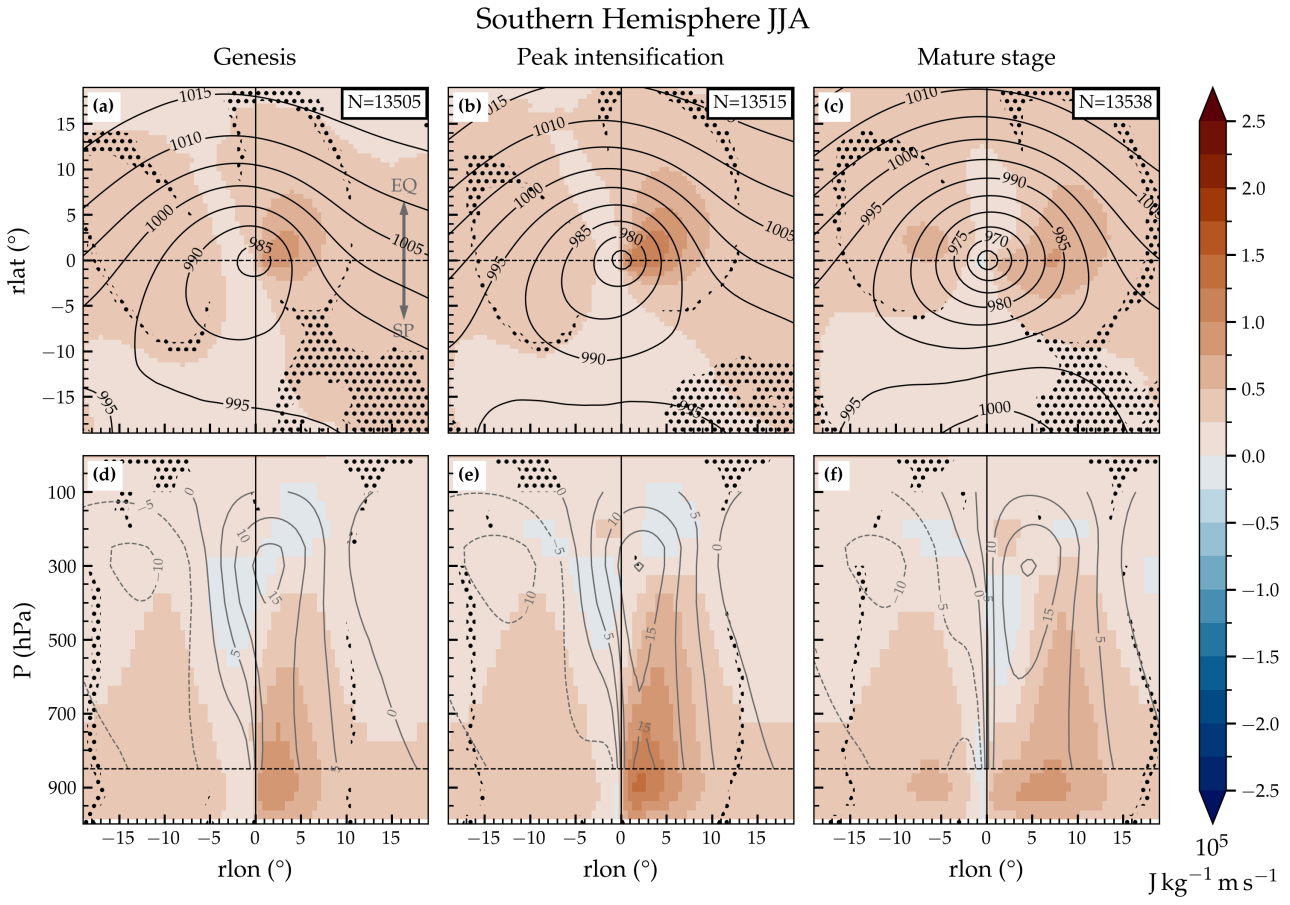

Figure C1. Statistical significance of composited TE MSE flux anomalies as in Fig. 3. Dotted areas indicate where the null hypothesis mean(SFA) = 0 (see Eq. C1) is not rejected at the 95 % confidence level. In **(d)–(f)**, grey contours indicate the (vertically sub-sampled) full meridional wind, v, as opposed to v' in Fig. 3d–f.

https://doi.org/10.5194/egusphere-2025-2314
Preprint. Discussion started: 30 May 2025

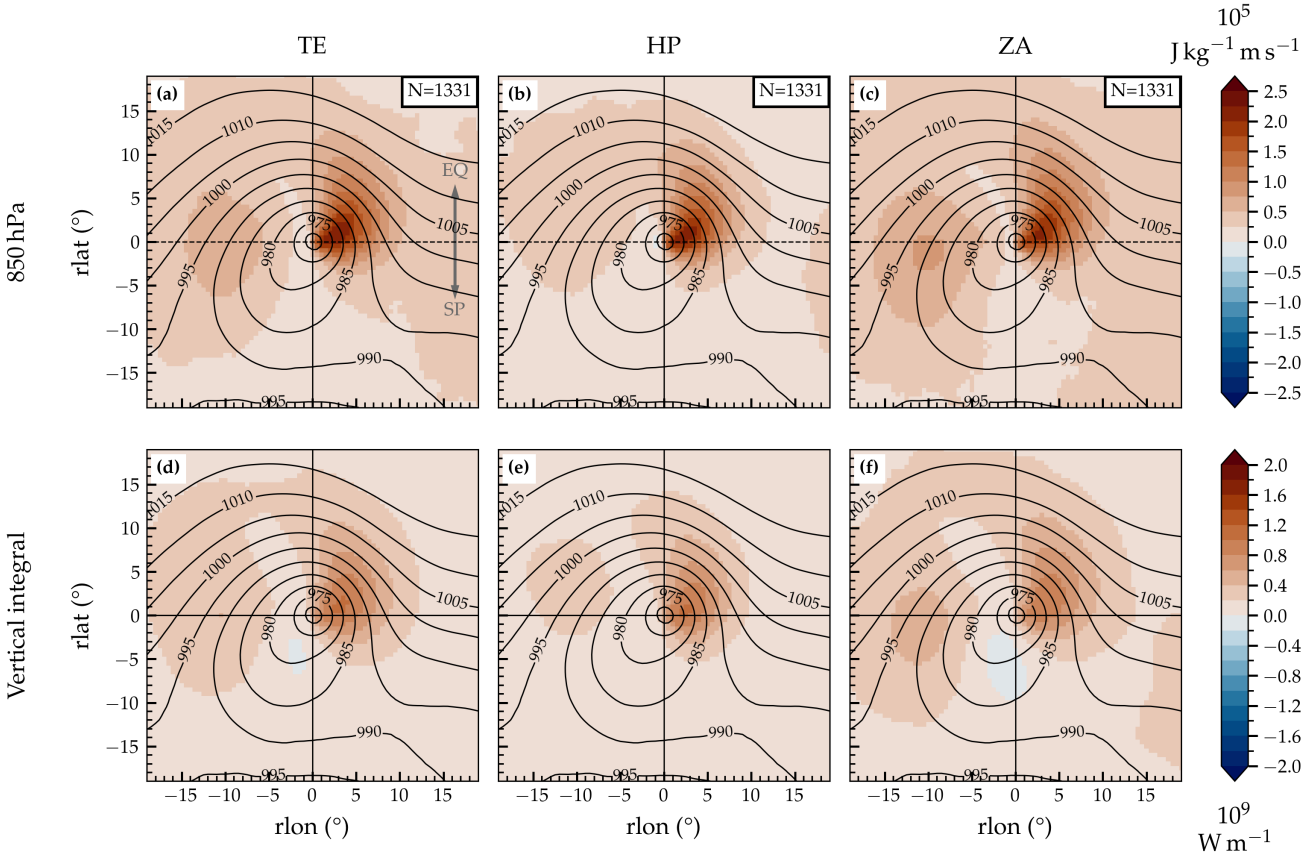

Figure C2. (a)–(c) Cyclone-centered eddy MSE flux at 850 hPa during time of maximum intensification for the 10 % most strongly intensifying SH cyclones during JJA for three different definitions of eddy flux (see method abbreviations in Sect. 1) in J m^{-1} kg s^{-1}. **(d)–(f)** Vertically integrated fluxes analogously to **(a)–(c)** but in units of W m^{-1}. Black contours indicate composite mean SLP in hPa. The number of cyclones in the composites are included in the upper right in panels **(a)–(c)**. A grey arrow is included for better orientation indicating directions of equator (EQ) and South Pole (SP).

https://doi.org/10.5194/egusphere-2025-2314
Preprint. Discussion started: 30 May 2025

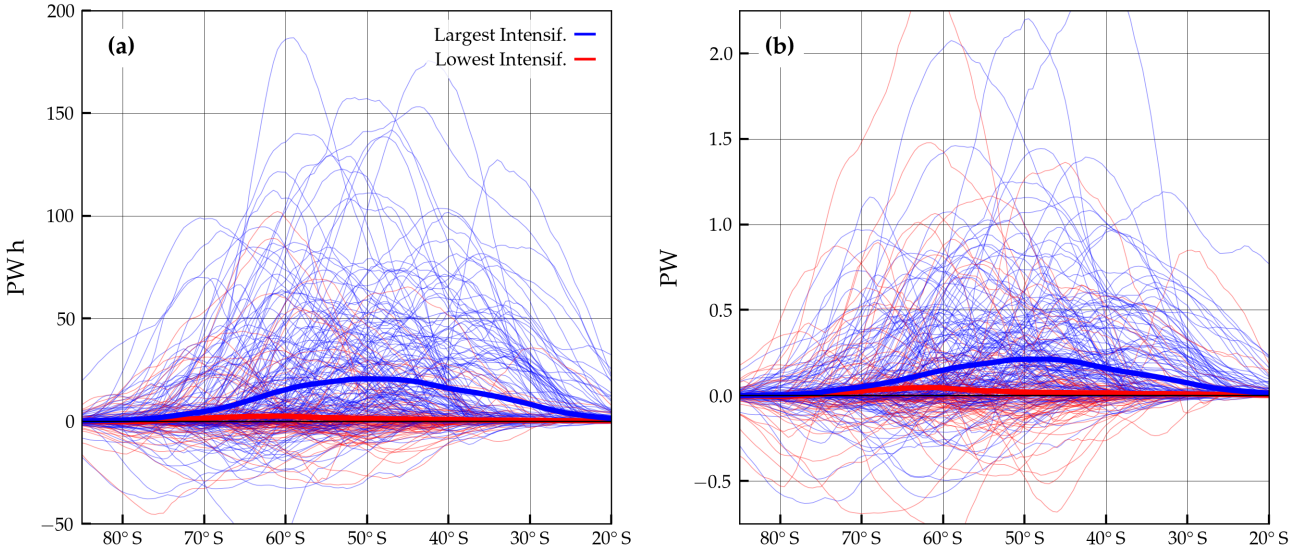

Figure D1. Zonally integrated TE MSE flux attributed to individual extratropical cyclones. **(a)** The lifetime-integrated flux (PW h) of the 200 most strongly intensifying cyclones (blue thin lines) is compared to the flux of the 200 cyclones that intensify least rapidly (red). Thick lines denote the arithmetic means shown in Fig. 8a. **(b)** As in **(a)** but for the lifetime-averaged flux in PW. The flux attribution percentile rank corresponds to 90 %.

https://doi.org/10.5194/egusphere-2025-2314
Preprint. Discussion started: 30 May 2025

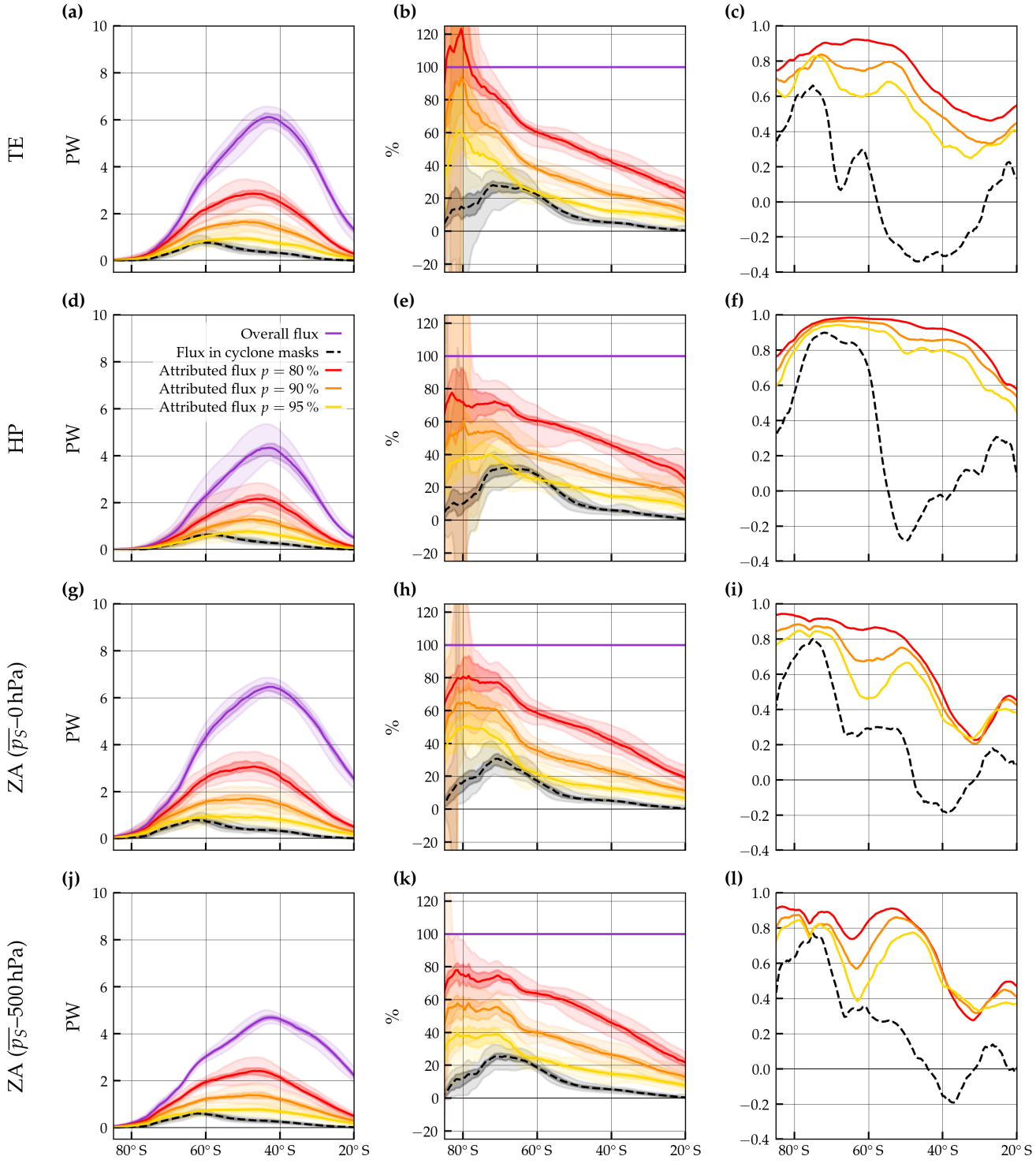

Figure D2. Same as Fig. 6 but repeated for different flux decomposition methods (see Sect. 2.3) and different percentile thresholds for attributing flux to cyclones (yellow, dark orange, and red distributions and lines corresponding to percentile ranks of 80, 90, and 95 %).

https://doi.org/10.5194/egusphere-2025-2314
Preprint. Discussion started: 30 May 2025

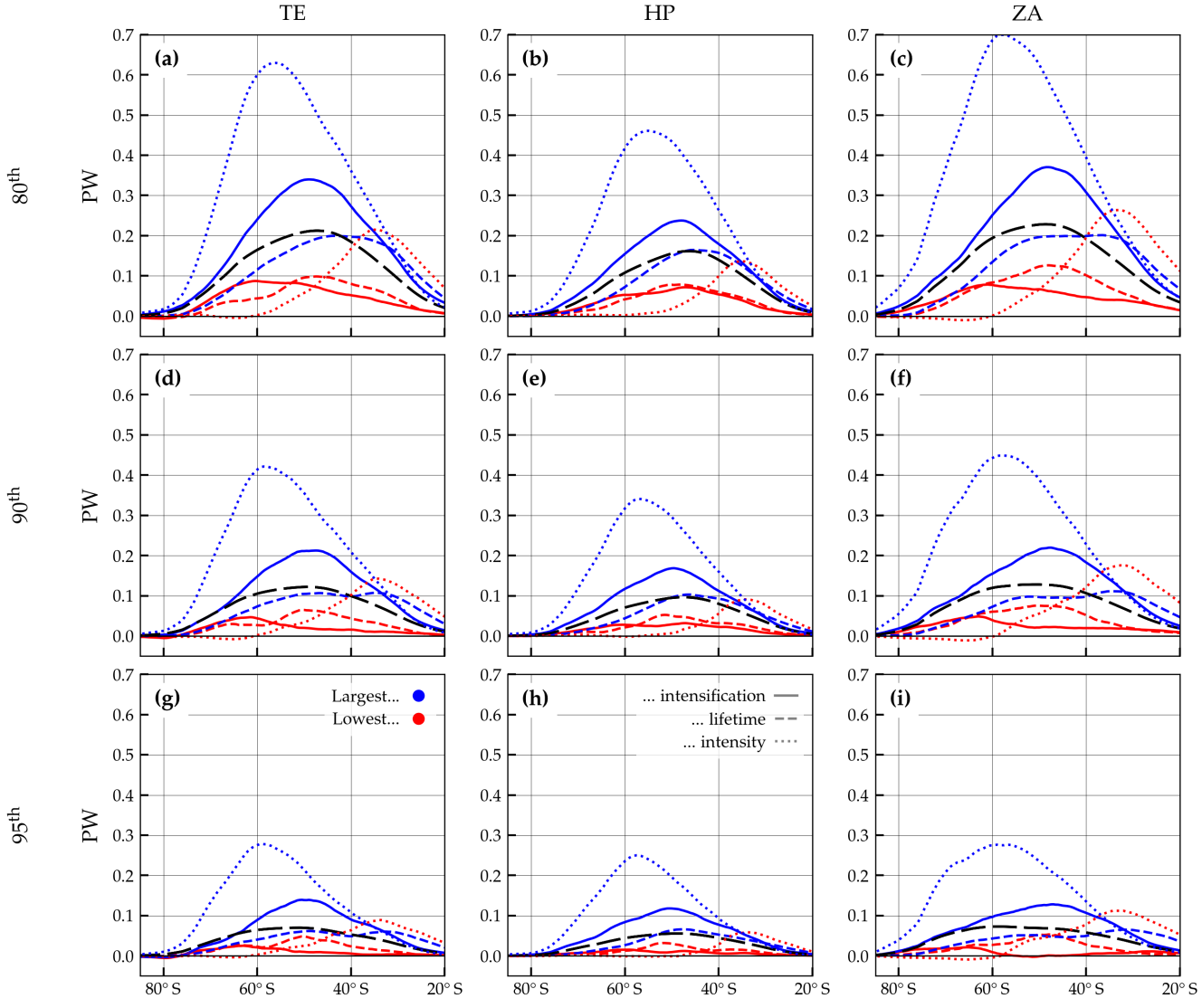

Figure D3. Sensitivity of cyclone-attributed averaged flux for all SH cyclones as in Fig. 8. Lines are equal to the ones in Fig. 8c for the different flux decomposition methods (see Sect. 2.3) and different flux percentile thresholds for attributing flux to cyclones (80, 90, and 95 %, see Sect. 2.5). The black dashed line represents the the average of all SH cyclones.

https://doi.org/10.5194/egusphere-2025-2314
Preprint. Discussion started: 30 May 2025

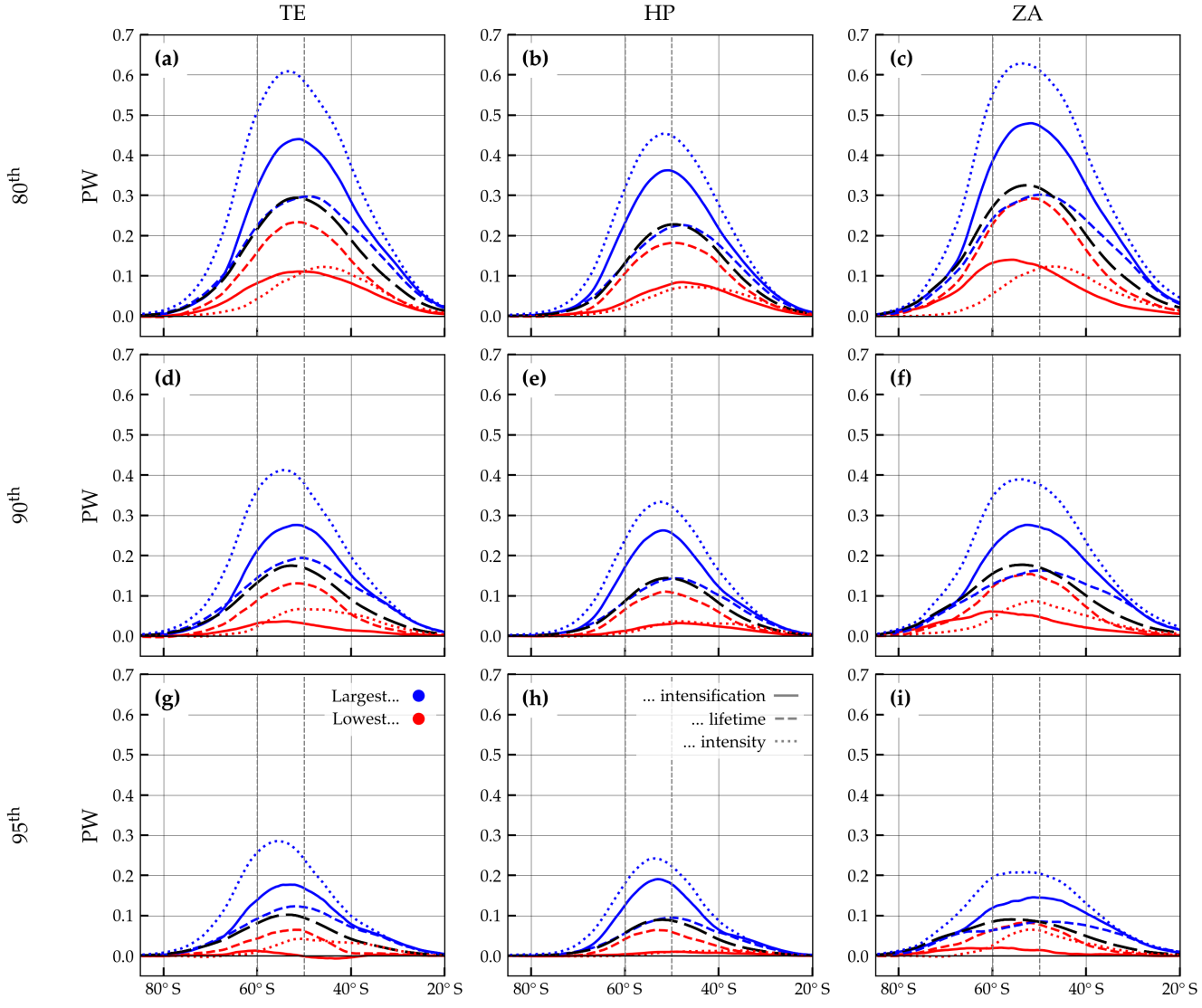

Figure D4. Cyclone-attributed TE MSE flux for cyclones that reach peak intensification between 50–60° S and have a minimum lifetime of 3 days as in Fig. 9c but repeated for different flux decomposition methods (columns, see Sect. 2.3) and different percentile thresholds for attributing flux to cyclones (80, 90, and 95 %. The black dashed line indicates the the arithmetic mean of all cyclones of that subset.

https://doi.org/10.5194/egusphere-2025-2314
Preprint. Discussion started: 30 May 2025

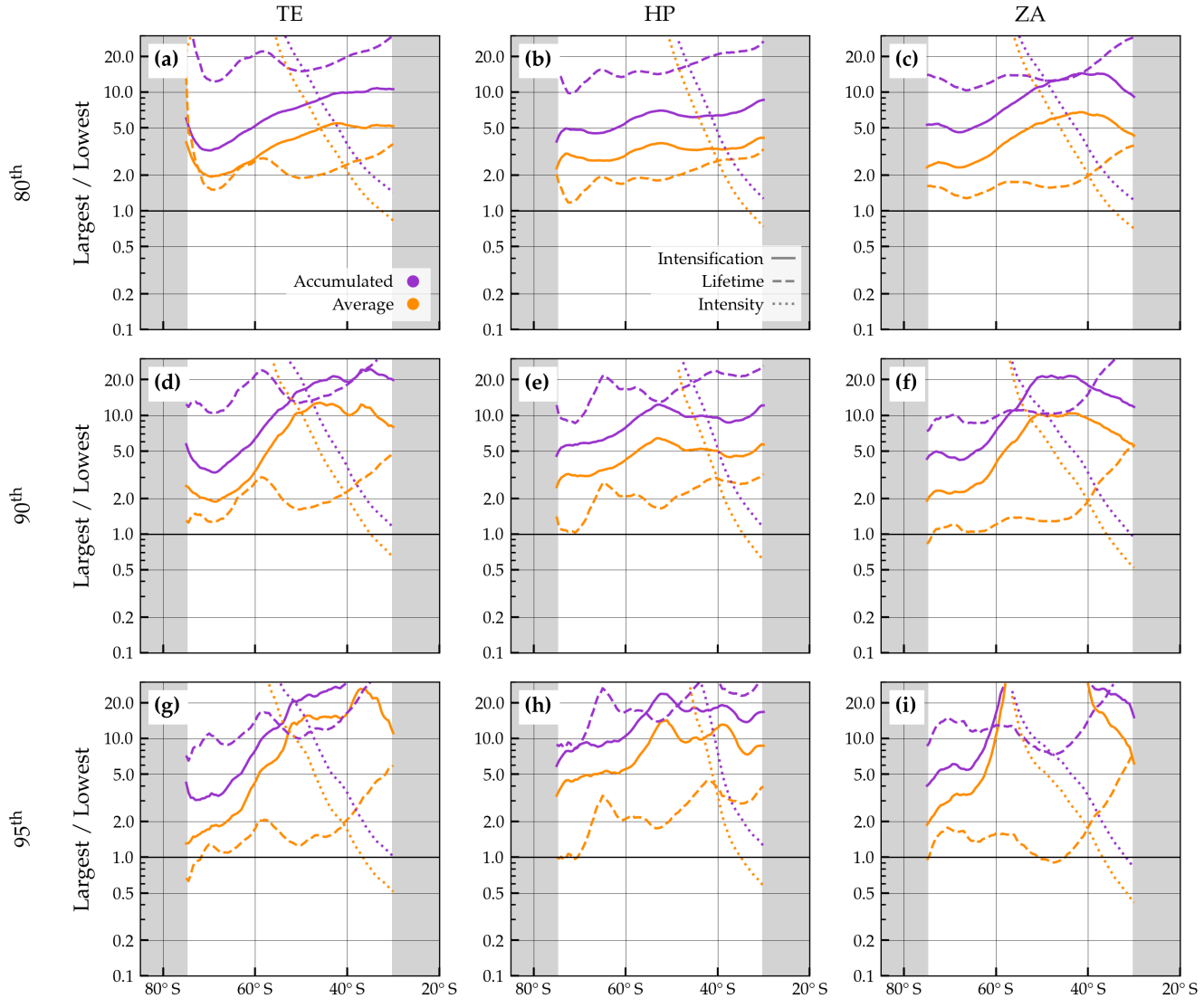

Figure D5. Ratio of the flux related to the 200 cyclones of largest vs. lowest characteristic based on all SH cyclones: Fig. 8b,d are combined and repeated for different flux decomposition methods (columns, see Sect. 2.3) and different percentile thresholds for attributing flux to cyclones (80, 90, and 95 %, see Sect. 2.5). Purple lines correspond to lifetime-accumulated fluxes, yellow lines to lifetime-averaged fluxes, and the linestyle signifies the cyclone life cycle characteristic.

https://doi.org/10.5194/egusphere-2025-2314
Preprint. Discussion started: 30 May 2025

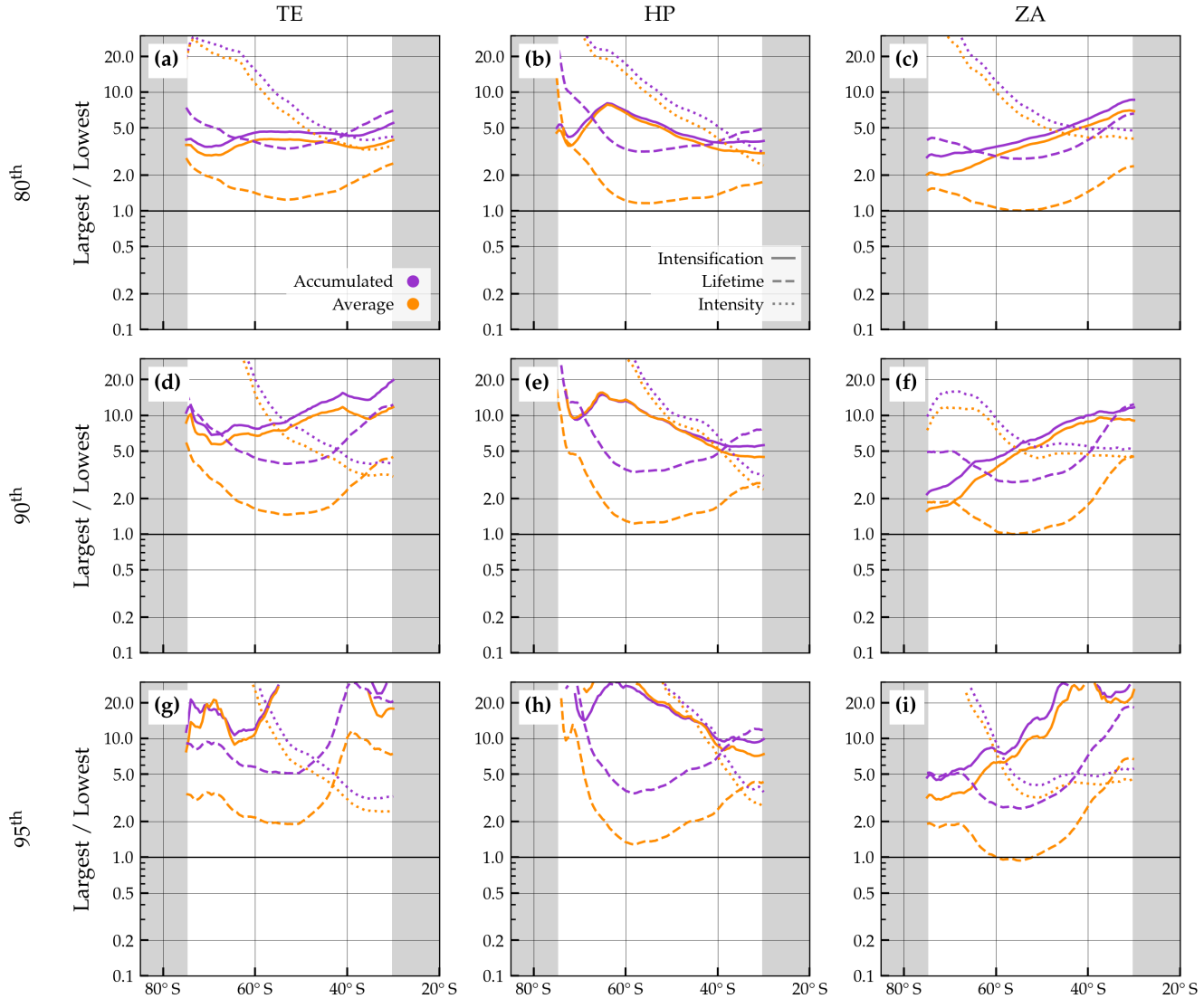

Figure D6. Ratio of the flux related to the 200 cyclones of largest vs. lowest life cycle characteristic (indicated by the line-style) based on the cyclones that pass 50°–60° S: Fig. 9b,d are reproduced for different flux decomposition methods (columns, see Sect. 2.3) and different percentile thresholds for attributing flux to cyclones (rows, see Sect. 2.5). Purple lines correspond to lifetime-accumulated fluxes and yellow lines to lifetime-averaged fluxes.

https://doi.org/10.5194/egusphere-2025-2314
Preprint. Discussion started: 30 May 2025

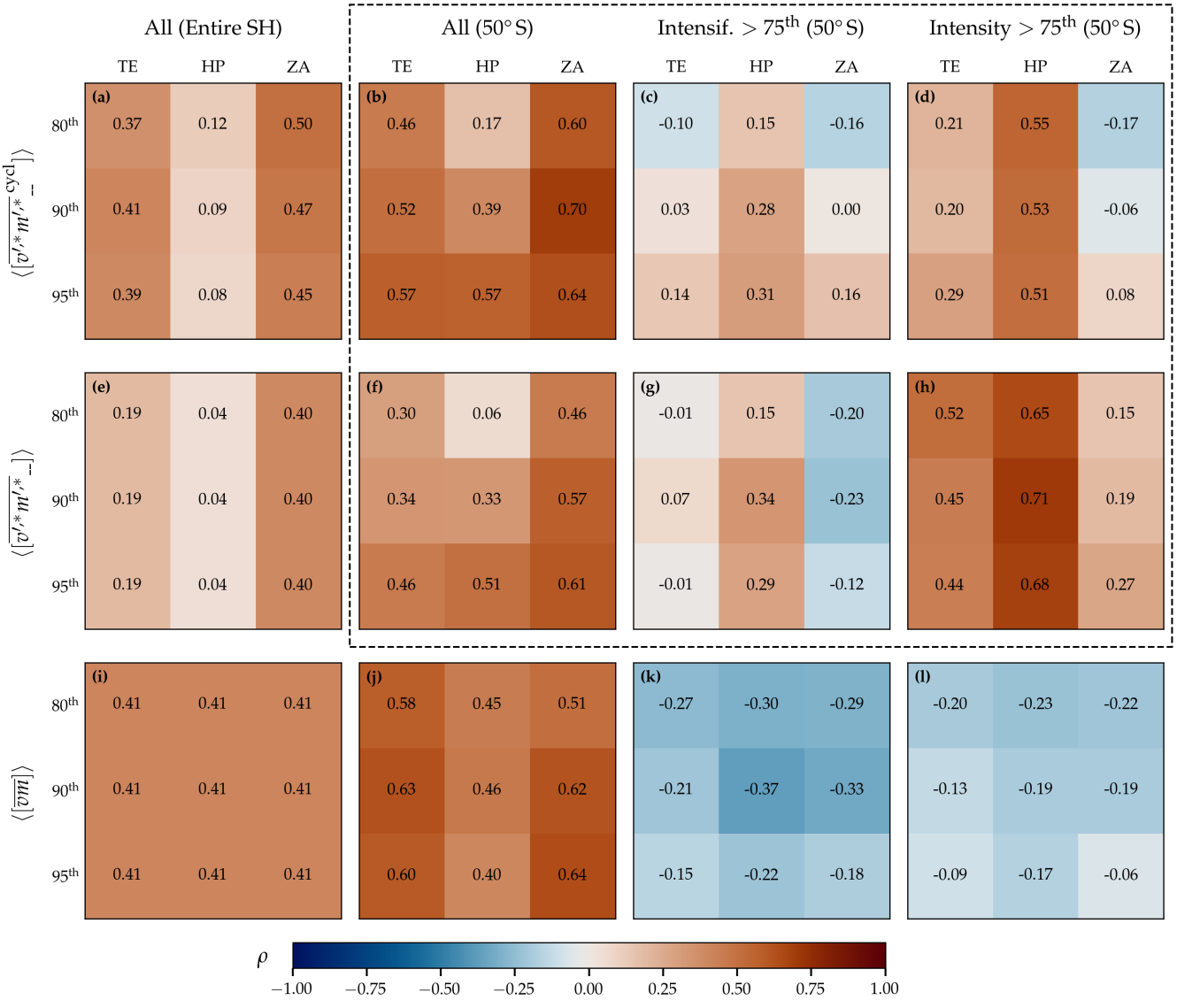

Figure E1. Sensitivity of the correlation (ρ) between seasonally averaged MSE fluxes and seasonal cyclone number to flux decomposition method and flux attribution percentile for different MSE fluxes and groups of cyclones. **(a)** The correlation of the number of all SH cyclones with cyclone-attributed eddy MSE flux, $\langle[\overline{v'^{,*}m'^{,*}}^{\text{cycl}}_{--}]\rangle$, at 50° S is shown for each percentile and flux decomposition method. Depending on the decomposition method, these fluxes correspond to temporal anomalies ($'$ for TE and HP) or zonal anomalies (* for ZA). Numerical values are accentuated with colors. Data correspond to SH JJA. This is repeated for **(b)** all cyclones with $\langle[\overline{v'^{,*}m'^{,*}}^{\text{cycl}}_{--}]\rangle \neq 0$ at 50° S, **(c)** the cyclones with $\langle[\overline{v'^{,*}m'^{,*}}^{\text{cycl}}_{--}]\rangle \neq 0$ at 50° S that have an intensification rate above the 75$^{\text{th}}$ climatological percentile, and **(d)** as **(c)** but for intensity instead of intensification rate. **(e–h)** as **(a–d)** but for the overall eddy MSE flux $\langle[\overline{v'^{,*}m'^{,*}}_{--}]\rangle$. **(i–l)** as **(a–d)** but for the total atmospheric MSE transport $\langle[\overline{vm}]\rangle$. The arrangement of the panels outlined by the black dashed line corresponds to the arrangement of the panels in Fig. 11.

https://doi.org/10.5194/egusphere-2025-2314
Preprint. Discussion started: 30 May 2025

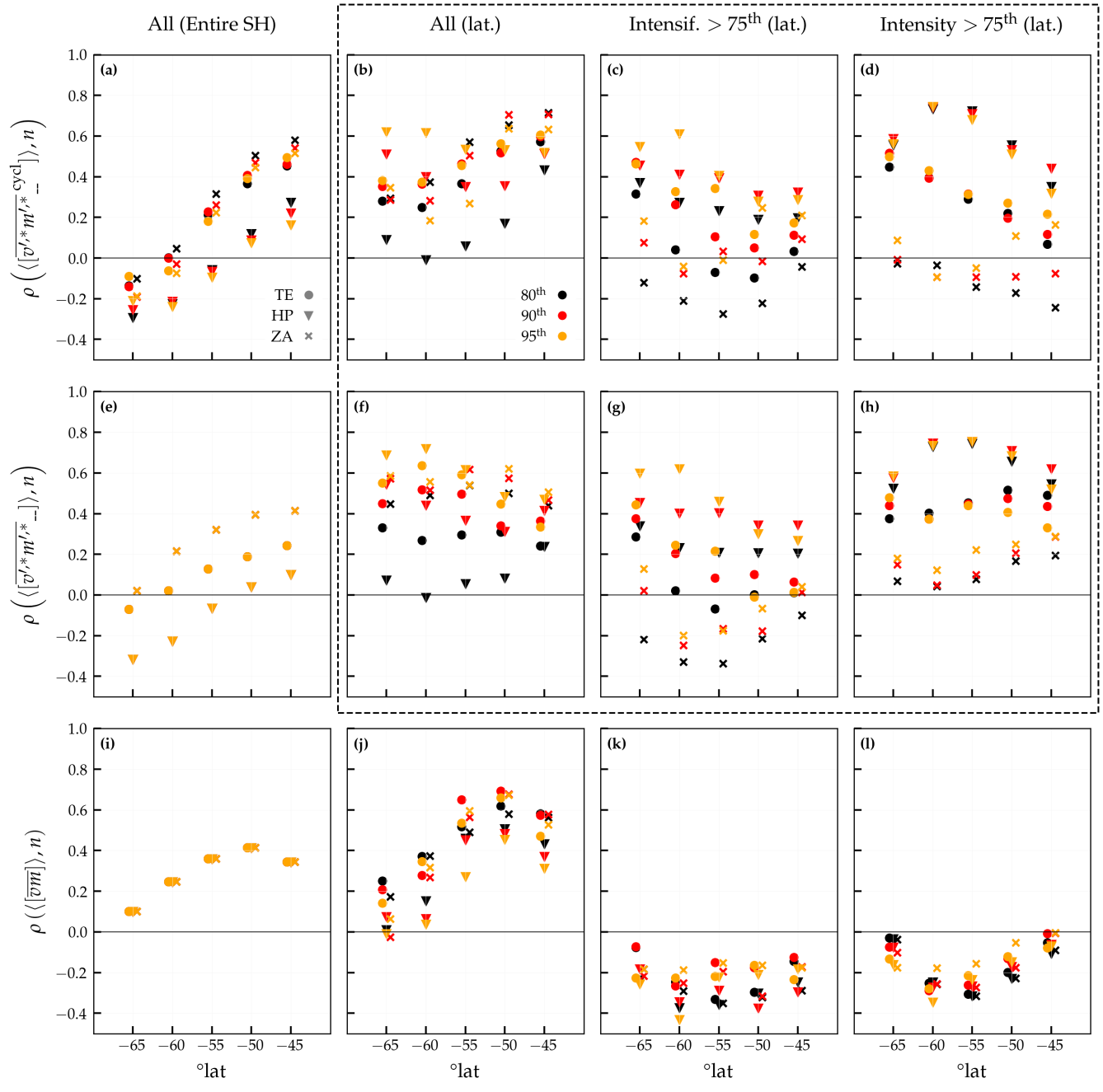

Figure E2. Sensitivity of the correlation (ρ) between seasonally averaged MSE fluxes and seasonal cyclone number to flux decomposition method and flux attribution percentile as in Fig. E1 for different latitudes. **(a)** As in Fig. E1a, the correlation of the number of all SH cyclones with cyclone-attributed eddy MSE flux, $\langle[\overline{v'^{,*}m'^{,*}}^{\mathrm{cycl}}_{--}]\rangle$, is shown here in steps of 5° latitude. Colors of the markers indicate the percentile and shapes the decomposition method. Markers for the different flux decomposition methods are slightly offset on the x-axis for better clarity. **(b–l)** as in **(a)** but for the different fluxes and groups of cyclones, arranged as in Fig. E1. The arrangement of the panels outlined by the black dashed line is consistent with Fig. 11.

https://doi.org/10.5194/egusphere-2025-2314
Preprint. Discussion started: 30 May 2025

Author contributions. SS conceived the project and acquired the funding. All authors contributed to the conceptualization of the study. JZ developed and implemented the methods, performed the data analysis, visualized the results, and prepared the original draft. AH supported assembling and maintaining ERA5 data. AH, AD, and SS contributed to the interpretation and discussion of the results and reviewed and edited the manuscript.

Competing interests. At least one of the (co-)authors is a member of the editorial board of Weather and Climate Dynamics.

Acknowledgements. We would like to acknowledge the Applied Physics Laboratory at the University of Washington for supporting a visit which greatly fostered scientific discussions regarding the results and outline of this work. We thank colleagues at the Institute for Atmospheric and Climate Science at ETH Zurich for constructive feedback. Furthermore, we would like to thank Heini Wernli for helpful discussions and feedback on the manuscript. The `cdo` library was used for data processing (Schulzweida, 2018). An AI-powered search engine was used for parts of code development (phind.com). J.Z., A.H., and S.S. were supported by the Swiss National Science Foundation through project grant Nr. 204181. A.D. was supported by the National Science Foundation Award AGS-2311154.

https://doi.org/10.5194/egusphere-2025-2314
Preprint. Discussion started: 30 May 2025

References

Armour, K. C., Siler, N., Donohoe, A., and Roe, G. H.: Meridional Atmospheric Heat Transport Constrained by Energetics and Mediated by Large-Scale Diffusion, J. Climate, 32, 3655–3680, https://doi.org/10.1175/JCLI-D-18-0563.1, 2019.

Barnes, E. A. and Hartmann, D. L.: The Global Distribution of Atmospheric Eddy Length Scales, J. Climate, 25, 3409–3416, https://doi.org/10.1175/JCLI-D-11-00331.1, 2012.

Barpanda, P. and Shaw, T.: Using the Moist Static Energy Budget to Understand Storm-Track Shifts across a Range of Time Scales, J. Atmos. Sci., 74, 2427–2446, https://doi.org/10.1175/JAS-D-17-0022.1, 2017.

Blanchard-Wrigglesworth, E., Cox, T., Espinosa, Z. I., and Donohoe, A.: The Largest Ever Recorded Heatwave—Characteristics and Attribution of the Antarctic Heatwave of March 2022, Geophys. Res. Lett., 50, e2023GL104 910, https://doi.org/10.1029/2023GL104910, 2023.

Boer, G. J. and Sargent, N. E.: Vertically Integrated Budgets of Mass and Energy for the Globe, J. Atmos. Sci., 42, 1592–1613, https://doi.org/10.1175/1520-0469(1985)042<1592:VIBOMA>2.0.CO;2, 1985.

Booth, J. F., Wang, S., and Polvani, L.: Midlatitude storms in a moister world: lessons from idealized baroclinic life cycle experiments, Clim. Dynam., 41, 787–802, https://doi.org/10.1007/s00382-012-1472-3, 2013.

Büeler, D. and Pfahl, S.: Potential Vorticity Diagnostics to Quantify Effects of Latent Heating in Extratropical Cyclones. Part I: Methodology, J. Atmos. Sci., 74, 3567–3590, https://doi.org/10.1175/JAS-D-17-0041.1, 2017.

Callaghan, J. and Power, S. B.: Major coastal flooding in southeastern Australia 1860-2012, associated deaths and weather systems, Aust. Meteorol. Ocean, 64, 183–213, https://doi.org/10.22499/2.6403.002, 2014.

Cardinale, C. J., Rose, B. E. J., Lang, A. L., and Donohoe, A.: Stratospheric and Tropospheric Flux Contributions to the Polar Cap Energy Budgets, J. Climate, 34, 4261–4278, https://doi.org/10.1175/JCLI-D-20-0722.1, 2021.

Catto, J. L., Shaffrey, L. C., and Hodges, K. I.: Can Climate Models Capture the Structure of Extratropical Cyclones?, J. Climate, 23, 1621–1635, https://doi.org/10.1175/2009JCLI3318.1, 2010.

Chang, E. K.: Projected Significant Increase in the Number of Extreme Extratropical Cyclones in the Southern Hemisphere, J. Climate, 30, 4915–4935, https://doi.org/10.1175/JCLI-D-16-0553.1, 2017.

Chang, E. K., Guo, Y., and Xia, X.: CMIP5 multimodel ensemble projection of storm track change under global warming, J. Geophys. Res.-Atmos., 117, 23 118, https://doi.org/10.1029/2012JD018578, 2012.

Chang, E. K. M.: CMIP5 Projected Change in Northern Hemisphere Winter Cyclones with Associated Extreme Winds, J. Climate, 31, 6527–6542, https://doi.org/10.1175/JCLI-D-17-0899.1, 2018.

Chikoore, H., Mbokodo, I. L., Singo, M. V., Mohomi, T., Munyai, R. B., Havenga, H., Mahlobo, D. D., Engelbrecht, F. A., Bopape, M. J. M., and Ndarana, T.: Dynamics of an extreme low temperature event over South Africa amid a warming climate, Weather and Climate Extremes, 44, 100 668, https://doi.org/10.1016/J.WACE.2024.100668, 2024.

Clark, J. P., Feldstein, S. B., and Lee, S.: Moist Static Energy Transport Trends in Four Global Reanalyses: Are They Downgradient?, Geophys. Res. Lett., 49, https://doi.org/10.1029/2022GL098822, 2022.

Cox, T., Donohoe, A., Armour, K. C., Frierson, D. M., and Roe, G. H.: Trends in Atmospheric Heat Transport Since 1980, J. Climate, 37, 1539–1550, https://doi.org/10.1175/JCLI-D-23-0385.1, 2024a.

Cox, T., Donohoe, A., Armour, K. C., Roe, G. H., and Frierson, D. M. W.: A New Method for Calculating Instantaneous Atmospheric Heat Transport, J. Climate, 37, 4337–4346, https://doi.org/10.1175/JCLI-D-23-0521.1, 2024b.

https://doi.org/10.5194/egusphere-2025-2314
Preprint. Discussion started: 30 May 2025

Dacre, H. F., Martinez-Alvarado, O., and Hodges, K. I.: Precipitation Efficiencies in a Climatology of Southern Ocean Extratropical Cyclones, J. Geophys. Res.-Atmos., 128, e2023JD039 239, https://doi.org/10.1029/2023JD039239, 2023.

Donohoe, A., Armour, K. C., Roe, G. H., Battisti, D. S., and Hahn, L.: The Partitioning of Meridional Heat Transport from the Last Glacial Maximum to CO2 Quadrupling in Coupled Climate Models, J. Climate, 33, 4141–4165, https://doi.org/10.1175/JCLI-D-19-0797.1, 2020.

Eady, E. T.: Long Waves and Cyclone Waves, Tellus, 1, 33–52, https://doi.org/10.3402/tellusa.v1i3.8507, 1949.

Fearon, M. G., Doyle, J. D., Ryglicki, D. R., Finocchio, P. M., and Sprenger, M.: The Role of Cyclones in Moisture Transport into the Arctic, Geophys. Res. Lett., 48, e2020GL090 353, https://doi.org/10.1029/2020GL090353, 2021.

Franzke, C. L. E. and Harnik, N.: Long-Term Trends of the Atmospheric Circulation and Moist Static Energy Budget in the JRA-55 Reanalysis, J. Climate, pp. 1–49, https://doi.org/10.1175/jcli-d-21-0724.1, 2023.

Fritsch, F. N. and Carlson, R. E.: Monotone Piecewise Cubic Interpolation, SIAM J. Numer. Anal., 17, 238–246, https://doi.org/10.1137/0717021, 1980.

Geen, R., Czaja, A., and Haigh, J. D.: The effects of increasing humidity on heat transport by extratropical waves, Geophys. Res. Lett., 43, 8314–8321, https://doi.org/10.1002/2016GL070214, 2016.

Geng, Q. and Sugi, M.: Possible Change of Extratropical Cyclone Activity due to Enhanced Greenhouse Gases and Sulfate Aerosols—Study with a High-Resolution AGCM, J. Climate, 16, 2262–2274, https://doi.org/10.1175/1520-0442(2003)16<2262:PCOECA>2.0.CO;2, 2003.

Gill, A. E.: Atmosphere—ocean dynamics, Academic Press, New York, 1982.

Grams, C. M., Wernli, H., Böttcher, M., Čampa, J., Corsmeier, U., Jones, S. C., Keller, J. H., Lenz, C. J., and Wiegand, L.: The key role of diabatic processes in modifying the upper-tropospheric wave guide: a North Atlantic case-study, Q.J. Roy. Meteor. Soc., 137, 2174–2193, https://doi.org/10.1002/QJ.891, 2011.

Grieger, J., Leckebusch, G. C., Donat, M. G., Schuster, M., and Ulbrich, U.: Southern Hemisphere winter cyclone activity under recent and future climate conditions in multi-model AOGCM simulations, Int. J. Climatol., 34, 3400–3416, https://doi.org/10.1002/JOC.3917, 2014.

Heitmann, K., Sprenger, M., Binder, H., Wernli, H., and Joos, H.: Warm conveyor belt characteristics and impacts along the life cycle of extratropical cyclones: case studies and climatological analysis based on ERA5, Weather Clim. Dynam., 5, 537–557, https://doi.org/10.5194/wcd-5-537-2024, 2024.

Hersbach, H., Bell, B., Berrisford, P., Hirahara, S., Horányi, A., Muñoz-Sabater, J., Nicolas, J., Peubey, C., Radu, R., Schepers, D., Simmons, A., Soci, C., Abdalla, S., Abellan, X., Balsamo, G., Bechtold, P., Biavati, G., Bidlot, J., Bonavita, M., Chiara, G., Dahlgren, P., Dee, D., Diamantakis, M., Dragani, R., Flemming, J., Forbes, R., Fuentes, M., Geer, A., Haimberger, L., Healy, S., Hogan, R. J., Hólm, E., Janisková, M., Keeley, S., Laloyaux, P., Lopez, P., Lupu, C., Radnoti, G., Rosnay, P., Rozum, I., Vamborg, F., Villaume, S., and Thépaut, J.: The ERA5 global reanalysis, Q.J. Roy. Meteor. Soc., 146, 1999–2049, https://doi.org/10.1002/qj.3803, 2020.

Hoskins, B. J., James, I. N., and White, G. H.: The Shape, Propagation and Mean-Flow Interaction of Large-Scale Weather Systems, J. Atmos. Sci., 40, 1595–1612, https://doi.org/10.1175/1520-0469(1983)040<1595:TSPAMF>2.0.CO;2, 1983.

Kang, J. M., Shaw, T. A., Kang, S. M., Simpson, I. R., and Yu, Y.: Revisiting the reanalysis-model discrepancy in Southern Hemisphere winter storm track trends, npj Clim. Atmos. Sci., 7, 1–10, https://doi.org/10.1038/s41612-024-00801-3, 2024.

Kaspi, Y. and Schneider, T.: The Role of Stationary Eddies in Shaping Midlatitude Storm Tracks, J. Atmos. Sci., 70, 2596–2613, https://doi.org/10.1175/JAS-D-12-082.1, 2013.

Kolstad, E. W. and Bracegirdle, T. J.: Marine cold-air outbreaks in the future: An assessment of IPCC AR4 model results for the Northern Hemisphere, Clim. Dynam., 30, 871–885, https://doi.org/10.1007/S00382-007-0331-0/FIGURES/10, 2008.

https://doi.org/10.5194/egusphere-2025-2314
Preprint. Discussion started: 30 May 2025

König, W., Sausen, R., and Sielmann, F.: Objective Identification of Cyclones in GCM Simulations, J. Climate, 6, 2217–2231, https://doi.org/10.1175/1520-0442(1993)006<2217:OIOCIG>2.0.CO;2, 1993.

Lambert, S. J. and Fyfe, J. C.: Changes in winter cyclone frequencies and strengths simulated in enhanced greenhouse warming experiments: Results from the models participating in the IPCC diagnostic exercise, Climate Dynamics, 26, 713–728, https://doi.org/10.1007/S00382-006-0110-3/TABLES/4, 2006.

Lembo, V., Fabiano, F., Galfi, V. M., Graversen, R. G., Lucarini, V., and Messori, G.: Meridional-energy-transport extremes and the general circulation of Northern Hemisphere mid-latitudes: dominant weather regimes and preferred zonal wavenumbers, Weather Clim. Dynam., 3, 1037–1062, https://doi.org/10.5194/wcd-3-1037-2022, 2022.

Lopez-Marti, F., Ginesta, M., Faranda, D., Rutgersson, A., Yiou, P., Wu, L., and Messori, G.: Future changes in compound explosive cyclones and atmospheric rivers in the North Atlantic, Earth Sys. Dynam., 16, 169–187, https://doi.org/10.5194/ESD-16-169-2025, 2025.

Marshall, J., Donohoe, A., Ferreira, D., and McGee, D.: The ocean's role in setting the mean position of the Inter-Tropical Convergence Zone, Clim. Dynam., 42, 1967–1979, https://doi.org/10.1007/s00382-013-1767-z, 2014.

Mayer, M., Kato, S., Bosilovich, M., Bechtold, P., Mayer, J., Schröder, M., Behrangi, A., Wild, M., Kobayashi, S., Li, Z., and L'Ecuyer, T.: Assessment of Atmospheric and Surface Energy Budgets Using Observation-Based Data Products, Surv. Geophys., pp. 1–28, https://doi.org/10.1007/S10712-024-09827-X/TABLES/5, 2024.

Messori, G. and Czaja, A.: On the sporadic nature of meridional heat transport by transient eddies, Q.J. Roy. Meteor. Soc., 139, 999–1008, https://doi.org/10.1002/qj.2011, 2013.

Messori, G. and Czaja, A.: Some considerations on the spectral features of meridional heat transport by transient eddies, Q.J. Roy. Meteor. Soc., 140, 1377–1386, https://doi.org/10.1002/QJ.2224, 2014.

Messori, G. and Czaja, A.: On local and zonal pulses of atmospheric heat transport in reanalysis data, Q.J. Roy. Meteor. Soc., 141, 2376–2389, https://doi.org/10.1002/qj.2529, 2015.

Messori, G., Geen, R., and Czaja, A.: On the spatial and temporal variability of atmospheric heat transport in a hierarchy of models, J. Atmos. Sci., 74, 2163–2189, https://doi.org/10.1175/JAS-D-16-0360.1, 2017.

Neelin, J. D. and Held, I. M.: Modeling Tropical Convergence Based on the Moist Static Energy Budget, Mon. Weather Rev., 115, 3–12, https://doi.org/10.1175/1520-0493(1987)115<0003:MTCBOT>2.0.CO;2, 1987.

Novak, L., Ambaum, M. H. P., and Tailleux, R.: The Life Cycle of the North Atlantic Storm Track, J. Atmos. Sci., 72, 821–833, https://doi.org/10.1175/JAS-D-14-0082.1, 2015.

Papritz, L., Pfahl, S., Rudeva, I., Simmonds, I., Sodemann, H., and Wernli, H.: The Role of Extratropical Cyclones and Fronts for Southern Ocean Freshwater Fluxes, J. Climate, 27, 6205–6224, https://doi.org/10.1175/JCLI-D-13-00409.1, 2014.

Peixoto, J. P. and Oort, A. H.: Physics of climate, American Institute of Physics, Melville, New York, 1992.

Pfahl, S. and Wernli, H.: Quantifying the Relevance of Cyclones for Precipitation Extremes, J. Climate, 25, 6770–6780, https://doi.org/10.1175/JCLI-D-11-00705.1, 2012.

Pfahl, S., Schwierz, C., Croci-Maspoli, M., Grams, C. M., and Wernli, H.: Importance of latent heat release in ascending air streams for atmospheric blocking, Nat. Geosci., 8, 610–614, https://doi.org/10.1038/ngeo2487, 2015.

Pomroy, H. R. and Thorpe, A. J.: The Evolution and Dynamical Role of Reduced Upper-Tropospheric Potential Vorticity in Intensive Observing Period One of FASTEX, Mon. Weather Rev., 128, 1817–1834, https://doi.org/10.1175/1520-0493(2000)128<1817:TEADRO>2.0.CO;2, 2000.

https://doi.org/10.5194/egusphere-2025-2314
Preprint. Discussion started: 30 May 2025

Priestley, C. H.: Heat transport and zonal stress between latitudes, Q.J. Roy. Meteor. Soc., 75, 28–40, https://doi.org/10.1002/qj.49707532307, 1949.

Priestley, M. D. K. and Catto, J. L.: Future changes in the extratropical storm tracks and cyclone intensity, wind speed, and structure, Weather Clim. Dynam., 3, 337–360, https://doi.org/10.5194/wcd-3-337-2022, 2022.

Rudeva, I. and Gulev, S. K.: Climatology of Cyclone Size Characteristics and Their Changes during the Cyclone Life Cycle, Mon. Weather Rev., 135, 2568–2587, https://doi.org/10.1175/MWR3420.1, 2007.

Ruggieri, P., Alvarez-Castro, M. C., Athanasiadis, P., Bellucci, A., Materia, S., and Gualdi, S.: North Atlantic Circulation Regimes and Heat Transport by Synoptic Eddies, J. Climate, 33, 4769–4785, https://doi.org/10.1175/JCLI-D-19-0498.1, 2020.

Rydsaa, J. H., Graversen, R. G., Heiskanen, T. I., and Stoll, P. J.: Changes in atmospheric latent energy transport into the Arctic: Planetary versus synoptic scales, Q.J. Roy. Meteor. Soc., 147, 2281–2292, https://doi.org/10.1002/QJ.4022, 2021.

Sanders, F. and Gyakum, J. R.: Synoptic-Dynamic Climatology of the "Bomb", Mon. Weather Rev., 108, 1589–1606, https://doi.org/10.1175/1520-0493(1980)108<1589:SDCOT>2.0.CO;2, 1980.

Schemm, S. and Rivière, G.: On the Efficiency of Baroclinic Eddy Growth and How It Reduces the North Pacific Storm-Track Intensity in Midwinter, J. Climate, 32, 8373–8398, https://doi.org/10.1175/JCLI-D-19-0115.1, 2019.

Schemm, S., Wernli, H., and Papritz, L.: Warm Conveyor Belts in Idealized Moist Baroclinic Wave Simulations, J. Atmos. Sci., 70, 627–652, https://doi.org/10.1175/JAS-D-12-0147.1, 2013.

Schemm, S., Sprenger, M., and Wernli, H.: When during Their Life Cycle Are Extratropical Cyclones Attended by Fronts?, B. Am. Meteorol. Soc., 99, 149–165, https://doi.org/10.1175/BAMS-D-16-0261.1, 2018.

Schemm, S., Papritz, L., and Rivière, G.: Storm track response to uniform global warming downstream of an idealized sea surface temperature front, Weather Clim. Dynam., 3, 601–623, https://doi.org/10.5194/wcd-3-601-2022, 2022.

Schulzweida, U.: CDO User Guide, https://doi.org/10.5281/ZENODO.1435455, 2018.

Seiler, C. and Zwiers, F. W.: How will climate change affect explosive cyclones in the extratropics of the Northern Hemisphere?, Clim. Dynam., 46, 3633–3644, https://doi.org/10.1007/S00382-015-2791-Y/FIGURES/6, 2016.

Shapiro, M. A. and Keyser, D.: Fronts, Jet Streams and the Tropopause, in: Extratropical Cyclones: The Erik Palmén Memorial Volume, edited by W., N. C. and Holopainen, E. O., pp. 167–191, American Meteorological Society, Boston, MA, ISBN 978-1-944970-33-8, https://doi.org/10.1007/978-1-944970-33-8_10, 1990.

Shaw, T. A., Barpanda, P., and Donohoe, A.: A Moist Static Energy Framework for Zonal-Mean Storm-Track Intensity, J. Atmos. Sci., 75, 1979–1994, https://doi.org/10.1175/JAS-D-17-0183.1, 2018.

Shields, C. A., Rutz, J. J., Leung, L. Y., Martin Ralph, F., Wehner, M., Kawzenuk, B., Lora, J. M., McClenny, E., Osborne, T., Payne, A. E., Ullrich, P., Gershunov, A., Goldenson, N., Guan, B., Qian, Y., Ramos, A. M., Sarangi, C., Sellars, S., Gorodetskaya, I., Kashinath, K., Kurlin, V., Mahoney, K., Muszynski, G., Pierce, R., Subramanian, A. C., Tome, R., Waliser, D., Walton, D., Wick, G., Wilson, A., Lavers, D., Prabhat, Collow, A., Krishnan, H., Magnusdottir, G., and Nguyen, P.: Atmospheric River Tracking Method Intercomparison Project (ARTMIP): Project goals and experimental design, Geosci. Model Dev., 11, 2455–2474, https://doi.org/10.5194/GMD-11-2455-2018, 2018.

Simmons, A. J.: Trends in the tropospheric general circulation from 1979 to 2022, Weather Clim. Dynam., 3, 777–809, https://doi.org/10.5194/wcd-3-777-2022, 2022.

Sinclair, M. R.: An Objective Cyclone Climatology for the Southern Hemisphere, Mon. Weather Rev., 122, 2239–2256, https://doi.org/10.1175/1520-0493(1994)122<2239:AOCCFT>2.0.CO;2, 1994.

https://doi.org/10.5194/egusphere-2025-2314
Preprint. Discussion started: 30 May 2025

Sinclair, V. A. and Dacre, H. F.: Which Extratropical Cyclones Contribute Most to the Transport of Moisture in the Southern Hemisphere?, J. Geophys. Res.-Atmos., 124, 2525–2545, https://doi.org/10.1029/2018JD028766, 2019.

Sinclair, V. A., Rantanen, M., Haapanala, P., Räisänen, J., and Järvinen, H.: The characteristics and structure of extra-tropical cyclones in a warmer climate, Weather Clim. Dynam., 1, 1–25, https://doi.org/10.5194/wcd-1-1-2020, 2020.

Sprenger, M., Fragkoulidis, G., Binder, H., Croci-Maspoli, M., Graf, P., Grams, C. M., Knippertz, P., Madonna, E., Schemm, S., Škerlak, B., and Wernli, H.: Global Climatologies of Eulerian and Lagrangian Flow Features based on ERA-Interim, B. Am. Meteorol. Soc., 98, 1739–1748, https://doi.org/10.1175/BAMS-D-15-00299.1, 2017.

Steinfeld, D., Boettcher, M., Forbes, R., and Pfahl, S.: The sensitivity of atmospheric blocking to upstream latent heating-numerical experiments, Weather Clim. Dynam., 1, 405–426, https://doi.org/10.5194/WCD-1-405-2020, 2020.

Stoll, P. J., Graversen, R. G., and Messori, G.: The global atmospheric energy transport analysed by a wavelength-based scale separation, Weather Clim. Dynam., 4, 1–17, https://doi.org/10.5194/WCD-4-1-2023, 2023.

Troup, A. J. and Streten, N. A.: Satellite-Observed Southern Hemisphere Cloud Vortices in Relation to Conventional Observations, J. Appl. Meteor., 11, 909–917, https://doi.org/10.1175/1520-0450(1972)011<0909:SOSHCV>2.0.CO;2, 1972.

Tsukernik, M. and Lynch, A. H.: Atmospheric Meridional Moisture Flux over the Southern Ocean: A Story of the Amundsen Sea, J. Climate, 26, 8055–8064, https://doi.org/10.1175/JCLI-D-12-00381.1, 2013.

Ullrich, P. A., Zarzycki, C. M., McClenny, E. E., Pinheiro, M. C., Stansfield, A. M., and Reed, K. A.: TempestExtremes v2.1: A community framework for feature detection, tracking, and analysis in large datasets, Geosci. Model Dev., 14, 5023–5048, https://doi.org/10.5194/GMD-14-5023-2021, 2021.

Vannière, B., Czaja, A., Dacre, H., Woollings, T., and Parfitt, R.: A potential vorticity signature for the cold sector of winter extratropical cyclones, Q.J. Roy. Meteor. Soc., 142, 432–442, https://doi.org/10.1002/QJ.2662, 2016.

Wernli, H. and Gray, S. L.: The importance of diabatic processes for the dynamics of synoptic-scale extratropical weather systems-a review, Weather Clim. Dynam., 5, 1299–1408, https://doi.org/10.5194/wcd-5-1299-2024, 2024.

Wernli, H. and Schwierz, C.: Surface Cyclones in the ERA-40 Dataset (1958–2001). Part I: Novel Identification Method and Global Climatology, J. Atmos. Sci., 63, https://doi.org/10.1175/JAS3766.1, 2006.

Wille, J. D., Alexander, S. P., Amory, C., Baiman, R., Barthélemy, L., Bergstrom, D. M., Berne, A., Binder, H., Blanchet, J., Bozkurt, D., Bracegirdle, T. J., Casado, M., Choi, T., Clem, K. R., Codron, F., Datta, R., Di Battista, S., Favier, V., Francis, D., Fraser, A. D., Fourré, E., Garreaud, R. D., Genthon, C., Gorodetskaya, I. V., González-Herrero, S., Heinrich, V. J., Hubert, G., Joos, H., Kim, S. J., King, J. C., Kittel, C., Landais, A., Lazzara, M., Leonard, G. H., Lieser, J. L., Maclennan, M., Mikolajczyk, D., Neff, P., Ollivier, I., Picard, G., Pohl, B., Ralph, F. M., Rowe, P., Schlosser, E., Shields, C. A., Smith, I. J., Sprenger, M., Trusel, L., Udy, D., Vance, T., Vignon, É., Walker, C., Wever, N., and Zou, X.: The Extraordinary March 2022 East Antarctica "Heat" Wave. Part I: Observations and Meteorological Drivers, J. Climate, 37, 757–778, https://doi.org/10.1175/JCLI-D-23-0175.1, 2024.

Zhang, Y. and Wang, W.-C.: Model-Simulated Northern Winter Cyclone and Anticyclone Activity under a Greenhouse Warming Scenario, J. Climate, 10, 1616–1634, https://doi.org/10.1175/1520-0442(1997)010<1616:MSNWCA>2.0.CO;2, 1997.

Zolina, O. and Gulev, S. K.: Synoptic Variability of Ocean–Atmosphere Turbulent Fluxes Associated with Atmospheric Cyclones, J. Climate, 16, 2717–2734, https://doi.org/10.1175/1520-0442(2003)016<2717:SVOOTF>2.0.CO;2, 2003.